Journal of Environmental Chemical Engineering 13 (2025) 115206

Contents lists available at ScienceDirect

Journal of Environmental Chemical Engineering

journal homepage: www.elsevier.com/locate/jece

Plastic waste-derived carbon nanotubes: Influence of growth catalyst and catalytic activity in CWPO

Fernanda F. Roman [a,b,c,*], Adriano S. Silva [a,b,c,d], Jose L. Diaz de Tuesta [e], Arthur P. Baldo [a,f], Jessica P.M. Lopes [a,g], Giane Gonçalves [g], Ana I. Pereira [d], Paulo Praça [h], Adrián M.T. Silva [b,c], Joaquim L. Faria [b,c], Manuel Bañobre-López [i], Helder T. Gomes [a,*]

[a] CIMO, LA SusTEC, Instituto Politécnico de Bragança, Campus de Santa Apolónia, Bragança 5300-253, Portugal
[b] LSRE-LCM – Laboratory of Separation and Reaction Engineering – Laboratory of Catalysis and Materials, Faculty of Engineering, University of Porto, Rua Dr. Roberto Frias, Porto 4200-465, Portugal
[c] ALiCE – Associate Laboratory in Chemical Engineering, Faculty of Engineering, University of Porto, Rua Dr. Roberto Frias, Porto 4200-465, Portugal
[d] CeDRI, SusTEC, Instituto Politécnico de Bragança, Campus de Santa Apolónia, Bragança 5300-253, Portugal
[e] Chemical and Environmental Engineering Group, ESCET, Universidad Rey Juan Carlos, C/ Tulipán s/n, Móstoles 28933, Spain
[f] Universidade Tecnológica Federal do Paraná (UTFPR), Campus Londrina, Av. dos Pioneiros, 3131 - Jardim Morumbi, Londrina, PR 86036-370, Brazil
[g] Universidade Tecnológica Federal do Paraná (UTFPR), Campus Ponta Grossa, Av. Monteiro Lobato, s/n km 04, Jardim Carvalho, Ponta Grossa 84016-210, Brazil
[h] Resíduos do Nordeste, EIM, S.A. Empresa Intermunicipal, Mirandela 5370-340, Portugal
[i] Advanced (Magnetic) Theranostic Nanostructures Lab, International Iberian Nanotechnology Laboratory, Av. Mestre Jose Veiga s/n, Braga 4715-330, Portugal

ARTICLE INFO

Keywords:
Plastic solid waste
Advanced oxidation processes (AOPs)
Heterogeneous Fenton
Acetaminophen
Contaminants of emerging concern
Carbocatalysts

ABSTRACT

Low-density polyethylene (LDPE) was used in this work to grow carbon nanotubes (CNTs) by chemical vapor deposition (CVD) over catalysts based on Ni, Fe and Al, synthesized either by co-precipitation (C) or wet impregnation (I) methods, with CNT yields in the range of 16–33 %. The morphology of the CNTs was directly influenced by the route used for the CVD catalyst synthesis, with co-precipitation-derived CVD catalysts resulting in CNT samples with curly walls. CNTs were purified with H_2SO_4 (10–50 *wt.*%) to remove attached metal particles. All synthesized materials (CVD-catalysts, as-synthesized CNTs, and purified CNTs) were tested as catalysts in the catalytic wet peroxide oxidation (CWPO) of paracetamol (PCM), chosen as a model pharmaceutical compound. Removals of 100 % of PCM in 8 h and 71 % of total organic carbon (TOC) in 24 h were achieved, with an H_2O_2 consumption efficiency of 76 % in 24 h for purified CNT (CNT@NiFeAl-C-P). The same CVD-catalyst (NiFeAl-C) was used to grow CNTs using real LDPE waste, and it was tested under the same reaction conditions, resulting in a PCM and TOC abatement of 90 % and 65 %, respectively. The synthesis of CNTs using LDPE waste was a good alternative, given the environmental benefits associated with its reintroduction into the economic cycle as a material with higher value than initially (upcycling).

1. Introduction

Plastic, derived mainly from petroleum-based hydrocarbons, encompasses a vast array of synthetic polymers common to numerous sectors, including packaging, construction, transportation, and healthcare. In 2021, 367 million tonnes of plastic were produced globally, with the European Union contributing significantly (*ca.* 30 %) [1]. Polyolefins, notably polypropylene and polyethylene, dominate the EU demand, especially in single-use packaging applications, leading to significant landfill accumulation [1]. This trend is projected to worsen, with terrestrial plastic accumulation forecasted to increase 2.8-fold by 2040, paralleled by a 2.6-fold increase in aquatic plastic pollution [2]. Current plastic management practices fail in alignment with a circular economy, and a combination of traditional and innovative solutions is required to drastically reduce PSW accumulation [1,3].

Recycling, whether mechanical or thermal, presents limitations such as polymer separation challenges and harmful emissions [3]. Chemical recycling offers a promising alternative by breaking down polymers into valuable monomers, enhancing the approach to circularity [4,5]. The high carbon content in most plastics makes them viable carbon sources to produce carbon-based materials like carbon nanotubes (CNTs), lowering feedstock costs and sustaining recycling attractiveness [6].

* Correspondence to: Instituto Politécnico de Bragança, Campus de Santa Apolónia, Bragança 5300-253, Portugal.
E-mail addresses: roman@ipb.pt (F.F. Roman), htgomes@ipb.pt (H.T. Gomes).

https://doi.org/10.1016/j.jece.2024.115206
Received 11 October 2024; Received in revised form 10 December 2024; Accepted 22 December 2024
Available online 24 December 2024

CNTs, synthesized predominantly via chemical vapor deposition (CVD), offer potential in catalytic processes, such as the catalytic wet peroxide oxidation (CWPO) [7]. CWPO relies on the selective formation of hydroxyl radicals ($HO^{\bullet}$) by the decomposition of hydrogen peroxide (H_2O_2) through the action of a suitable catalyst [8], resulting in the non-selective degradation of organic compounds present in the wastewater [9].

Several catalysts have been studied for CWPO purposes [10–14], with CNTs being active and stable heterogeneous catalysts in this application [11,15]. In the early stages, the catalysts used for CWPO purposes had transition metals in their structure [16]. Later, the literature started reporting the use of carbonaceous materials as an alternative to iron-based ones to tackle their limitations, *e.g.* metal leaching [13]. Despite the recognized carbon catalyst activity towards CWPO, most works using CNTs do not differentiate if the activity comes from the metals introduced on the CNTs, the residual metals from the synthesis procedure, or from the carbonaceous phase [16–18]. In most cases, acid washing (*i.e.*, using HNO_3, HCl, or H_2SO_4) is used to remove metals coming from the CVD procedure that are present in the CNTs, removing amorphous carbon, and further leading to introducing oxygen surface groups during this process. Nevertheless, the influence of acid washing is rarely explored. Furthermore, most papers dealing with CNTs from actual PSW focus mostly on their synthesis (Figure S1); and to determine whether these materials are equivalent to traditional CNTs requires studying their application. In addition, there is little to no comparison between the materials prepared using dirty and clean PSW, which is of utmost importance for the process scalability.

This paper addresses these gaps by focusing on CNTs synthesized from low-density polyethylene (LDPE), a common plastic waste constituent, and applying the CNTs in the CWPO of paracetamol (PCM, also known as acetaminophen), which is a pharmaceutical compound that has been found in different water matrixes, including drinking water [19]. By evaluating both as-synthesized and purified CNTs, with varying acid purification degrees, the study aims to elucidate their efficacy in degrading PCM, removing total organic carbon (TOC), and consuming H_2O_2. Furthermore, CNTs were synthesized with real cleaned and dirty PSW composed of LDPE from a municipal solid waste management facility and tested as catalysts as a proof-of-concept.

2. Experimental procedure and methods

The description of reagents and materials used in the present work is shown in Text S1.

2.1. Materials synthesis and characterization

2.1.1. Synthesis of catalysts for chemical vapour deposition (CVD)

Catalysts for CVD were synthesized by two methods (wet impregnation or co-precipitation) depositing 20 % of the active phase (Ni and/or Fe) onto the support (D20 Katalyst), following previously described procedures [20,21]. In the case of the wet impregnation method, a solution containing the metal precursor (Ni or Ni/Fe) was mixed with 4 g of support, and the water in excess was evaporated using a rotary evaporator, resulting in the Ni-Al_2O_3-I and NiFe-Al_2O_3-I samples, respectively. For the co-precipitation method, the metal precursors (Ni/Fe) and support were mixed, and the metal oxides were precipitated by dropwise addition of $NH_4(OH)$ until reaching a pH 8 (sample NiFe-Al_2O_3-C). An additional sample was produced by direct co-precipitation of Ni, Fe and Al (no support added), labeled as NiFeAl-C. All these samples were dried in an oven at 60 °C for 24 h and calcined in air at 850 °C for 3 h. The yield of metallic nanoparticles was calculated using Eq. (1) [20,21]:

$$Yield(wt.\%) = \frac{\%MO}{\%MO_{theoretical}} \quad (1)$$

where *%MO* is the percentual of metal oxides obtained after synthesis (calculated with data from the digestion of the samples) and $\%MO_{theoretical}$ is the theoretical percentual of metallic nanoparticles.

2.1.2. Synthesis of carbon nanotubes (CNTs)

The oven (TH/TV, Termolab) used in the synthesis of the CNTs consists of three regions with independent temperature controllers (T_1, T_2 and T_3), as shown elsewhere [11]. The oven was set up by loading 1 g of CVD-catalyst in a crucible in the lower region (T_3) and 5 g of LDPE in a crucible in the upper region (T_1). The synthesis was carried out at T_1 = 450 °C and T_3 = 850 °C with 1 h hold time when reaching the desired temperature under N_2 atmosphere (100 mNL min^{-1}). The temperature was set to 850 °C to ensure the formation of CNTs, following the results reported in a previous work [22]. The obtained CNTs were named as follows: *CNT@CVD-catalyst*, according to the CVD-catalyst used (*i.e.*, CNT@Ni-Al_2O_3-I, CNT@NiFe-Al_2O_3-I, CNT@NiFe-Al_2O_3-C, and CNT@NiFeAl-C). The yield of the CNTs was calculated according to Eq. (2):

$$Yield(wt.\%) = \frac{m_{recovered} * (1 - \%ashes)}{m_{LDPE} * 0.865} \quad (2)$$

where m_{LDPE} is the mass of LDPE loaded in the reactor at the beginning of the CVD process (in g), $m_{recovered}$ is the mass of material recovered at the end of the CVD process (in g), and *%ashes* is the content of ashes of the as-synthesized CNTs (in *wt.*%), determined by TGA analysis.

After synthesis, a fraction of the CNTs was subjected to acid washing to remove the metal catalyst (50 % v/v H_2SO_4, 140 °C, 3 h, under reflux), as described elsewhere [23]. After cooling to room temperature, the material was thoroughly washed with distilled water until reaching the neutrality of the rising waters, giving origin to purified CNTs (**P** included after the name). The material was dried in oven at 60 °C overnight, leading to CNT@Ni-Al_2O_3-I-P, CNT@NiFe-Al_2O_3-I-P, CNT@NiFe-Al_2O_3-C-P, and CNT@NiFeAl-C-P. CNT@NiFeAl-C was also subjected to acid washing considering different concentrations of H_2SO_4 (10 and 30 % v/v) for 3 h at 140 °C, leading to CNT@NiFeAl-C-P-10 and CNT@NiFeAl-C-P-30, respectively. The mass yield after acid washing was determined by Eq. (3):

$$Yield(wt.\%) = 1 - \frac{m_{CNT-P}}{m_{CNT}} \quad (3)$$

where m_{CNT-P} is the mass of purified CNTs after washing (in g) and m_{CNT} is the mass of CNTs before washing (in g).

As a proof-of-concept, a run was also carried out with a sample separated from the PSW supplied by Resíduos do Nordeste, EIM SA. Figure S2 displays the FTIR spectrum of this sample, the typical bands ascribed to LDPE being confirmed (2921 and 2853 cm^{-1} for asymmetrical and symmetrical, respectively stretching of -CH_2, 1474 and 1464 cm^{-1} for bending deformation, 1375 cm^{-1} for CH_3 symmetric deformation, and 721 cm^{-1} for rocking deformation [24]). The LDPE derived from PSW was washed with water to remove the dirt particles attached to its surface, and the CVD process was carried out under the same conditions as explained above (considering NiFeAl-C as CVD catalyst). The recovered material was purified with H_2SO_4, as previously described, leading to CNT_R-W@NiFeAl-C-P. The as-received LDPE sample (AR) from PSW was also directly used (without washing) as carbon precursor for the preparation of CNTs (once again considering NiFeAl-C as CVD catalyst). The recovered material was purified with H_2SO_4 as abovementioned (50 % v/v H_2SO_4, 140 °C, 3 h, under reflux), leading to CNT_R-AR@NiFeAl-C-P.

The detailed description of the characterization techniques can be found in Text S2 [25]. Briefly, SEM/EDS and TEM were used to characterize the as-synthesized CNTs. N_2 adsorption-desorption isotherms were used to study the textural properties of CNTs. The magnetic properties of CNTs were studied using SQUID. Moreover, TGA and FTIR were used to characterize the surface chemistry and thermogravimetric

properties of the materials. The hydrophobicity/hydrophilicity was also estimated by determining the drop contact angles. XRD of the metal substrates was obtained to analyze crystal compositions.

2.2. Catalytic wet peroxide oxidation (CWPO)

Catalytic wet peroxide oxidation (CWPO) was carried out for all the materials synthesized in this work (both metallic or carbonaceous), namely: (i) **CVD-catalysts** used for the growth of CNTs (to evaluate their contribution towards the CWPO reaction), (ii) **as-synthesized CNTs** still bearing the catalysts used during CVD reaction, and (iii) the **purified CNTs** with reduced metal content. CWPO was conducted by adapting a procedure described elsewhere [10]. Briefly, 100 mL of a PCM solution with a concentration of $[PCM]_0 = 100$ mg L^{-1} at pH 3.5 (previously adjusted by employing H_2SO_4 1 M and/or NaOH 1 M) was loaded into a reaction vessel and submerged into an oil bath equipped with temperature control (C-MAG HS 7, IKA) and a condenser. The reaction vessel was heated to 80 ºC. Upon reaching the desired temperature, the stoichiometric amount of H_2O_2 (30 % w/v) needed to fully degrade PCM was added ($[H_2O_2]_0 = 474$ mg L^{-1}), followed by the catalyst at a concentration of $c_{catalyst} = 2.5$ g L^{-1}, considering this time $t_0 = 0$ min. The reaction was monitored at pre-determined intervals (0, 15, 30, 60, 120, 240, 360, 480 and 1440 min) by analyzing TOC, PCM and H_2O_2 concentration. Metal leaching, aromatic compounds (ARM) and total phenolic content (TP) were determined at the end of the reaction. Both pristine and purified CNTs were tested on the CWPO of PCM. Adsorption runs were conducted in the same conditions ($pH_0 = 3.5$, $c_{adsorbent} = 2.5$ g L^{-1}, $[PCM]_0 = 100$ mg L^{-1} and 80 ºC) and PCM concentration was measured after 24 h of contact time by UV-Vis at 246 nm. A non-catalytic run (N.C.) was also assessed under the same conditions in the absence of catalyst. By the end of the reaction, the catalyst was separated from the reaction medium, dried at 60 °C overnight. For reutilization runs, the dried recovered catalyst was directly used in a new CWPO reaction following the procedure described above, adjusting the volume of the reaction to achieve a catalyst concentration of 2.5 g L^{-1} (no fresh catalyst added).

Some experiments of PCM desorption from the CNTs were conducted for 6 h at room temperature using a solution composed of 0.5 M NaOH and ethanol (20 %) at a CNT concentration of 1.5 g L^{-1}, adapting a procedure described elsewhere [26]. The analytical techniques carried out to determine PCM, H_2O_2, TOC during the reactions and metal leaching (*i.e.* Ni and Fe) are described in Text S3, Equation S1 and Figure S3 [10,27].

3. Results and discussion

3.1. Materials characterization

3.1.1. Metal content and yields

Table 1 presents the yields of synthesized materials and their Ni, Fe, and ashes contents. CVD-catalysts achieved 88–92 % incorporation of metallic particles, calculated based on Eq. (1). CNT@Ni-Al_2O_3-I prepared by wet impregnation resulted in the lowest yield of CNTs (16 *wt.*%), while CNT@NiFeAl-C obtained by co-precipitation had the highest (33 *wt.*%). Yao *et al.* (2018) also reported lower yields with a Ni-based catalyst obtained via wetness impregnation compared to a co-precipitation-derived catalyst from plastic waste steam reforming [28]. Higher yields correlated with lower ashes contents, CNT@Ni-Fe-Al_2O_3-C and CNT@NiFeAl-C displaying higher yields (33 and 23 *wt.*%, respectively) and lower ashes contents (12.1 and 39.9 *wt.*%, respectively). Ashes content decreased significantly (45–93 %) after purification (purified CNT in Table 1), the ashes content of the purified samples only being higher than 6.0 *wt.*% for CNT@Ni-Al_2O_3-I-P (*i.e.*, 14.2 *wt.*%). Acid concentration (H_2SO_4, 10, 30 or 50 % v/v) during washing affected metal particle removal, with the lower concentration (10 % v/v) yielding 5.5 *wt.*% ashes and higher concentrations yielding 3.0–5.5 *wt.*%.

CNT@Ni-Al_2O_3-I had the highest Ni content (5.4 *wt.*%), while as-synthesized NiFe-Al_2O_3 based CNTs had similar Ni (1.7 %) and Fe (4.6–4.7 %) contents. Acid washing reduced these metal contents by 63–88 %, resulting in materials with 0.3–1.7 % of Fe and 0.2–1.7 % of Ni. Alumina-supported CNTs (CNT@Ni-Al_2O_3-I-P, CNT@NiFe-Al_2O_3-I-P, CNT@NiFe-Al_2O_3-C-P) showed a greater decrease in ashes content (71–93 %) compared to individual metallic particles (65–71 %) after purification, indicating more pronounced removal of alumina.

3.1.2. Morphology of the obtained CNTs

The as-synthesized CNTs obtained from pure LDPE were characterized by SEM, and some micrographs are shown in Fig. 1. It is possible to observe the formation of filamentous carbonaceous structures regardless of the CVD catalyst used. Metal particles can be seen in all images (bright spots on the SEM micrographs). All purified CNTs were observed via TEM, and some micrographs are displayed in Fig. 2. In all cases, as expected, residual metallic particles were still observed, mainly within the

Table 1
Contents of ashes, Ni and Fe on the CVD-catalysts and CNTs and yields.

Material	Type	Fe (*wt.*%)	Ni (*wt.*%)	Ashes (*wt.*%)	Organic content[¥] (*wt.*%)	Yield (%)
Ni-Al_2O_3-I	CVD-catalyst	-	10.1	100	0	92[a]
NiFe-Al_2O_3-I		8.3	4.5	100	0	88[a]
NiFe-Al_2O_3-C		8.9	4.5	100	0	90[a]
NiFeAl-C		15.3	9.3	100	0	89[a]
CNT@Ni-Al_2O_3-I	As-synthesized CNT	-	5.4	49.9	50.1	16[b]
CNT@NiFe-Al_2O_3-I		4.7	1.7	39.9	60.1	23[b]
CNT@NiFe-Al_2O_3-C		4.6	1.7	52.3	47.7	18[b]
CNT@NiFeAl-C		2.5	0.9	12.1	87.9	33[b]
CNT_R-W@NiFeAl-C		ND	ND	ND	ND	25[b]
CNT_R-AR@NiFeAl-C		ND	ND	ND	ND	22[b]
CNT@Ni-Al_2O_3-I-P	Purified CNT	-	1.7 (−68 %[d])	14.2 (−71 %[d])	85.8	42.3[c]
CNT@NiFe-Al_2O_3-I-P		0.8 (−83 %[d])	0.2 (−71 %[d])	3.2 (−92 %[d])	96.8	49.3[c]
CNT@NiFe-Al_2O_3-C-P		1.7 (−63 %[d])	0.6 (−65 %[d])	3.8 (−93 %[d])	96.2	48.3[c]
CNT@NiFeAl-C-P		0.3 (−88 %[d])	0.3 (−66 %[d])	3.7 (−71 %[d])	96.3	55.3[c]
CNT@NiFeAl-C-P−30		0.3(−88 %[d])	0.2 (−78 %[d])	3.0 (−75 %[d])	97.0	54.0[c]
CNT@NiFeAl-C-P−10		0.3(−88 %[d])	0.3 (−66 %[d])	5.5 (−45 %[d])	94.5	67.0[c]
CNT_R-W@NiFeAl-C-P		0.4	0.3	3.5	96.5	51.1[c]
CNT_R-AR@NiFeAl-C-P		0.4	0.4	3.7	96.3	48.4[c]
CNT-C	Commercial sample	0.4	-	2.0	98.0	-

¥ Organic content = 100 – ashes (*wt.*%); [a]calculated according to Eq. (1); [b]calculated according to Eq. (2); and [c]yield after purification stage calculated according to Eq. (3);[d]variation of the parameter in relation to its parent material. ND = not determined.

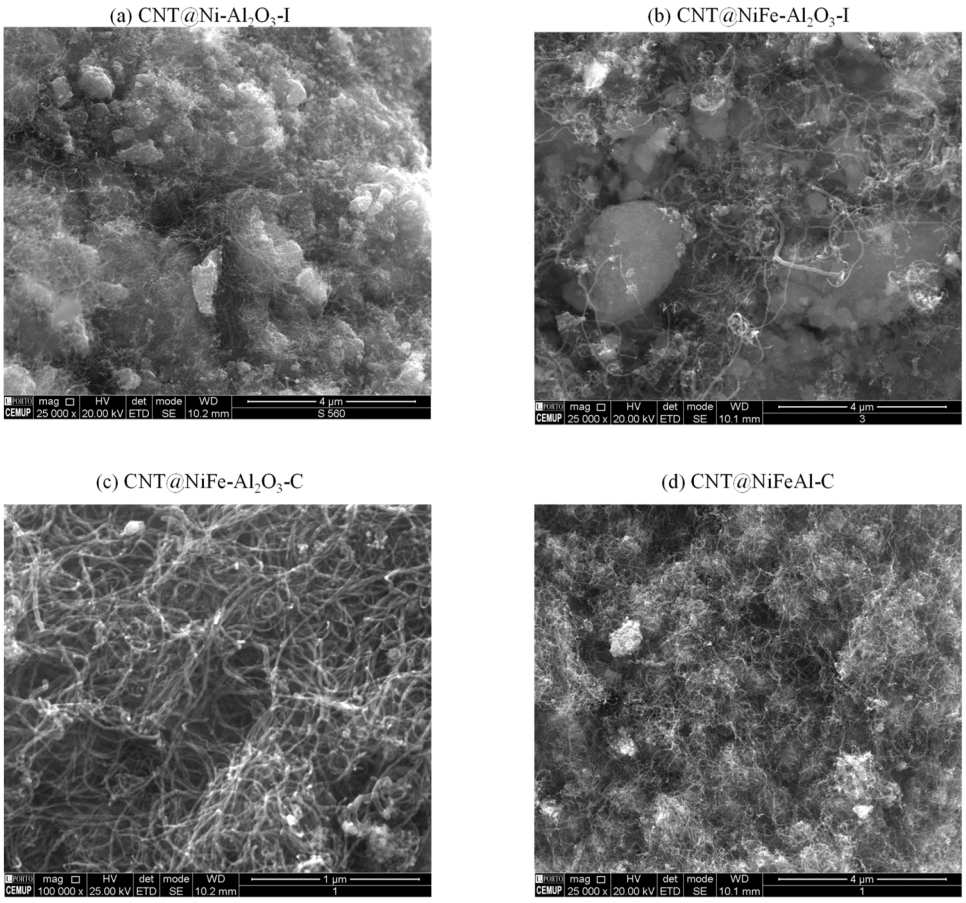

Fig. 1. SEM images of (a) CNT@Ni-Al_2O_3-I, (b) CNT@NiFe-Al_2O_3-I, (c) CNT@NiFe-Al_2O_3-C and (d) CNT@NiFeAl-C.

CNT structure. The destruction of the sample would be required to remove metallic particles completely. CNT@Ni-Al_2O_3-I-P (Fig. 2(a-b)) displays hollow filamentous structures, mainly with a linear structure. On the other hand, CNT@NiFe-Al_2O_3-I-P (Fig. 2(c-d)) has a more defectuous structure. CNT@NiFe-Al_2O_3-C-P (Fig. 2(e-f)) is mainly formed by curly tubes, which seem to arise from multiple growing events, and some of the fibers seem filled with amorphous carbon structures. Long hollow tubes were observed in CNT@NiFeAl-C-P (Fig. 2 (g-h)), and some were curly. The samples obtained from LDPE wastes as precursors (CNT_R-W@NiFeAl-C-P and CNT_R-AR@NiFeAl-C-P, *i.e.* respectively using washed and as-received samples in the CVD process) were also formed by long hollow tubes (Fig. 2(i-j) and (k-l), respectively), with more defects on their structure when compared to the sample produced with pure LDPE (visually observed).

In Figure S4, the distribution of outer diameters estimated for the CNTs using imageJ are represented. Higher average diameters are observed for CNT@NiFe-Al_2O_3-I-P (16.3 nm, Figure S4 (b)), with some fibers with diameters in the range of 60–100 nm. The remaining CNTs display a more limited diameter range (5–45 nm, Figure S4). CNT@NiFe-Al_2O_3-C-P resulted in the lowest average diameter (11.5 nm, Figure S4 (c)), and CNT@NiFeAl-C-P is the material with the narrowest diameter distribution (5–30 nm, Figure S4 (d)). The materials prepared from LDPE waste also resulted in similar diameters. CNT_R-W@NiFeAl-C-P resulted in an average of 17.0 nm (Figure S4 (e)) whereas CNT_R-AR@NiFeAl-C-P (Figure S4 (f)) resulted in an average of 16.2 nm. For all CNTs, carbon interlaying spacing was ~0.34 nm, which is the expected value for CNTs [29].

Comparing directly CNT@NiFe-Al_2O_3-I-P and CNT@NiFe-Al_2O_3-C-P, which differ only in the technique used to prepare these catalysts, a wide difference is observed in terms of average diameter and distribution of diameters. In the case of CNT@NiFe-Al_2O_3-I-P, a larger diameter is observed, and especially, large particles were found (>60 nm) (Figure S4 (b)). In the case of CNT@NiFe-Al_2O_3-C-P, the average diameter is much lower, and the range of particles is much narrower (5–45 nm, Figure S4 (c)). Wet impregnation was reported to result in a much higher average diameter of Ni particles when compared with other synthesis methods [28], mainly related to its poor dispersion over the support, and poor distribution of metallic particles has been correlated with the growth of CNTs with larger diameters [30,31], which may explain the results observed here.

3.1.3. *Textural and thermogravimetric properties*

N_2 adsorption/desorption isotherms were obtained for CVD-catalysts and CNT samples (Figure S5-S8), with results summarized in Table 2. Among the CVD-catalysts, NiFeAl-C (the catalyst without support) exhibited the lowest surface area (106 $m^2\ g^{-1}$) and pore volume (181 $mm^3\ g^{-1}$). Materials supported on alumina showed surface areas of 130–138 $m^2\ g^{-1}$ and pore volumes of 350–429 $mm^3\ g^{-1}$, indicating pore obstruction of the alumina (pure alumina had surface area of 185 $m^2\ g^{-1}$ and a pore volume of 437 $mm^3\ g^{-1}$). NiFe-Al_2O_3-I catalyst had slightly lower surface area (130 $m^2\ g^{-1}$) and total pore volume (375 $mm^3\ g^{-1}$) compared to NiFe-Al_2O_3-C (138 $m^2\ g^{-1}$ and 429 $mm^3\ g^{-1}$, respectively). Consistent surface area and pore volume results for Ni-based catalysts prepared via co-precipitation or wetness impregnation were previously documented [28]. CNT growth positively affected surface area for higher yield materials (CNT@NiFe-Al_2O_3-I, 18 % increase; CNT@NiFeAl-C, 42 % increase). Conversely, CNT@Ni-Al_2O_3-I experienced a significant decrease in surface area and pore volume (from 131 to 72 $m^2\ g^{-1}$), possibly due to CNT growth within catalyst pores.

Acid washing had minimal effects on surface area except for CNT@Ni-Al_2O_3-I, which increased by 300 % (*i.e.*, up to 226 $m^2\ g^{-1}$). The purification process leads to a minimal increase in surface area for

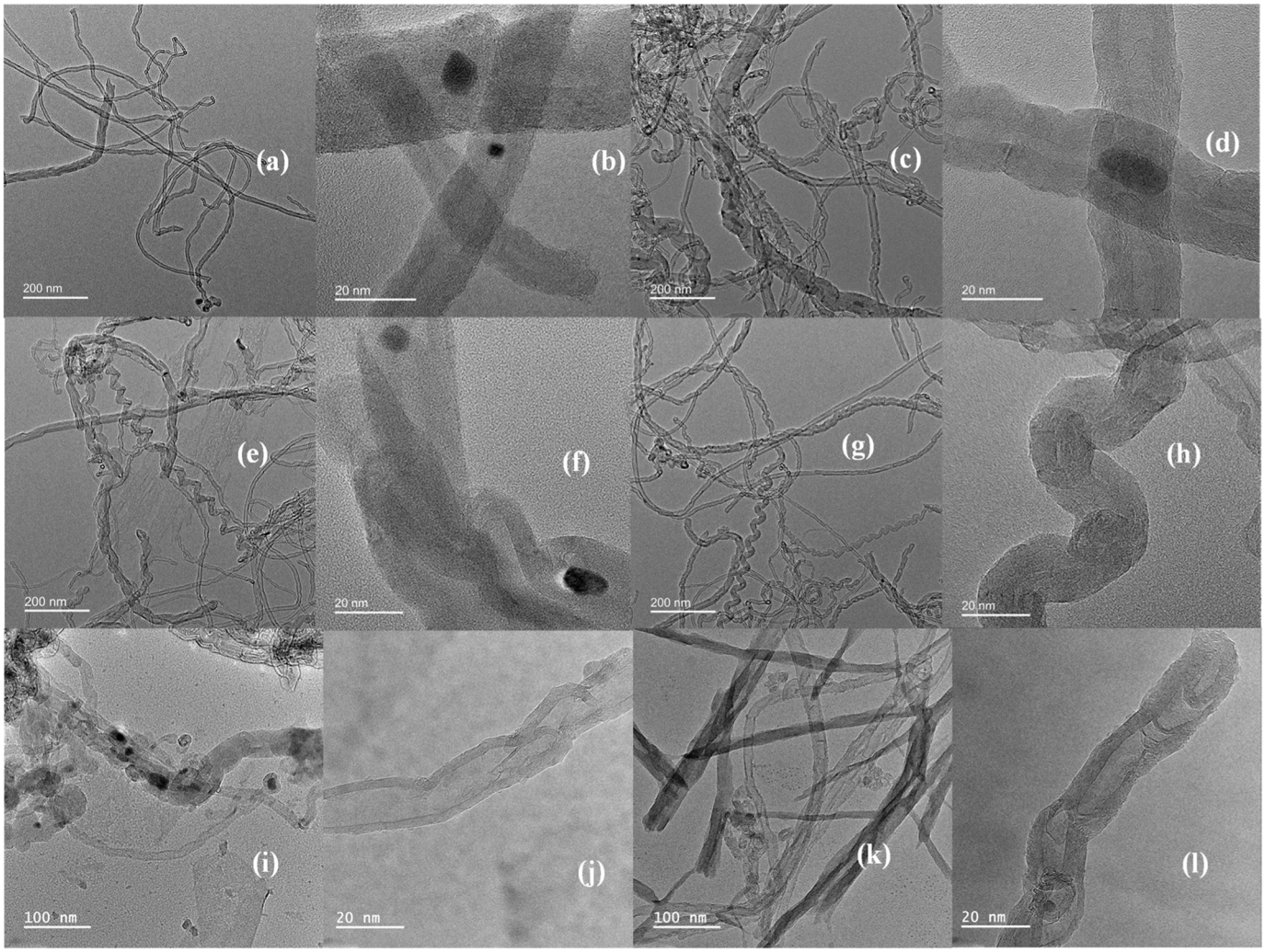

Fig. 2. TEM images of (a-b) CNT@Ni-Al_2O_3-I-P, (c-d) CNT@NiFe-Al_2O_3-I-P, (e-f) CNT@NiFe-Al_2O_3-C-P, and (g-h) CNT@NiFeAl-C-P, (i-j) CNT_R-W@NiFeAl-C-P and (k-l) CNT_R-AR@NiFeAl-C-P.

Table 2
Comparison of S_{BET} and total pore volume (V_{total}) of the CVD-catalysts, the as-synthesized CNTs and purified CNTs.

Material	Type	S_{BET} ($m^2\ g^{-1}$)	V_{total} ($mm^3\ g^{-1}$)
Al_2O_3	Support	185	437
Ni-Al_2O_3-I	CVD-catalyst	131	350
NiFe-Al_2O_3-I		130	375
NiFe-Al_2O_3-C		138	429
NiFeAl-C		106	181
CNT@Ni-Al_2O_3-I	As-synthesized CNT	72	168
CNT@NiFe-Al_2O_3-I		153	431
CNT@NiFe-Al_2O_3-C		134	415
CNT@NiFeAl-C		151	422
CNT@Ni-Al_2O_3-I-P	Purified CNT	226	608
CNT@NiFe-Al_2O_3-I-P		155	574
CNT@NiFe-Al_2O_3-C-P		161	578
CNT@NiFeAl-C-P		153	444
CNT_R-W@NiFeAl-C-P		160	597
CNT_R-AR@NiFeAl-C-P		186	654
CNT-C	Commercial sample	254	690

two pristine carbon nanotubes (CNTs), namely CNT@NiFe-Al_2O_3-I and CNT@NiFeAl-C, with ash contents of 39.9 *wt.*% and 12.1 *wt.*% respectively. Samples from LDPE waste exhibited higher surface areas (CNTR-W@NiFeAl-C-P: 160 $m^2\ g^{-1}$, CNTR-AR@NiFeAl-C-P: 186 $m^2\ g^{-1}$) compared to pure LDPE-derived sample (153 $m^2\ g^{-1}$), possibly due to more defective structure formation [32]. A commercial sample of CNTs used here for comparison purposes showed a surface area of 254 $m^2\ g^{-1}$ and a pore volume of 690 $mm^3\ g^{-1}$, consistent with typical multiwalled CNT surface areas (10–500 $m^2\ g^{-1}$).

Fig. 3 displays TGA (left Y-axis, black) and DTG (right Y-axis, yellow) curves for both as-synthesized and purified CNTs. The initiation (mass loss) temperature for as-synthesized CNTs (Fig. 3(a-d)) ranges from approximately 400 to 460 °C, while for purified CNTs (Fig. 3(e-h)) the values are higher (between 480 and 530 °C). The presence of some amorphous carbon is suggested by mass loss below 410 °C in as-synthesized CNTs [33]. Purification removes the amorphous carbon, enhancing stability against oxidation. Higher initiation temperatures in purified CNTs are attributed to reduced metallic particle content, which catalyzes decomposition [32]. A study linked Ni particle content to initiation temperature, indicating decreased stability with higher Ni content [34].

DTG profiles determine the oxidation temperature, reflecting CNT stability towards oxidation [35]. Lower temperatures suggest defect sites [35]. Among the as-synthesized samples, CNT@NiFeAl-C exhibits the highest oxidation temperature (702 °C, Fig. 3(d)), followed by CNT@NiFe-Al_2O_3-I (692 °C, Fig. 3(b)), CNT@Ni-Al_2O_3-I (657 °C, Fig. 3(a)), and CNT@NiFe-Al_2O_3-C (622 °C, Fig. 3(c)). Lower ashes content in CNT@NiFeAl-C (12.1 *wt.*%, Table 1) explains its higher oxidation and initiation temperatures. After purification, most samples show narrower

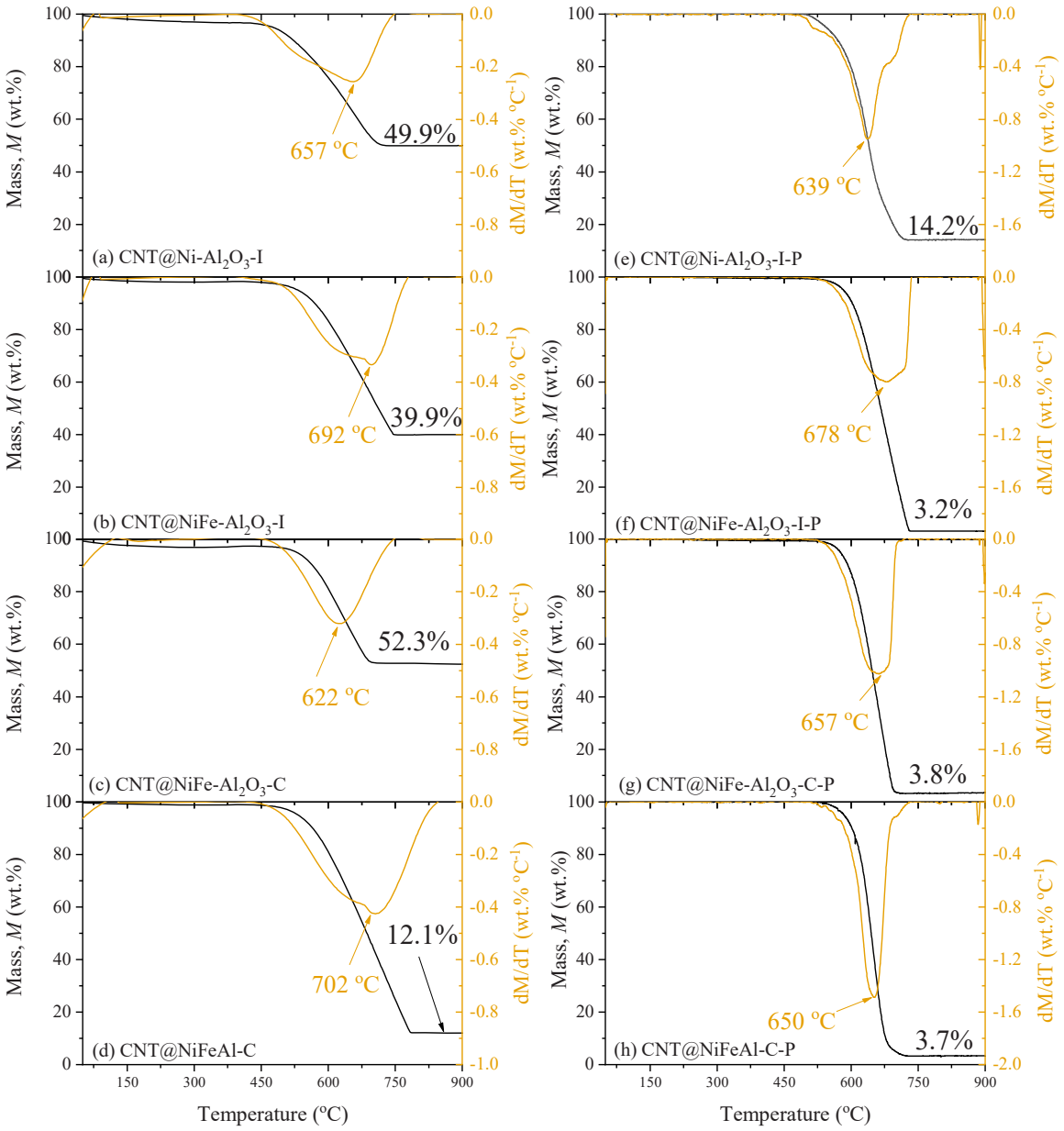

Fig. 3. Thermogravimetric analysis (left axis, black) and DTG curves (right axis, yellow) of as-synthesized (a-d) and purified (e-h) CNTs: (a) CNT@Ni-Al_2O_3-I, (b) CNT@NiFe-Al_2O_3-I, (c) CNT@NiFe-Al_2O_3-C,(d) CNT@NiFeAl-C, (e) CNT@Ni-Al_2O_3-I-P, (f) CNT@NiFe-Al_2O_3-I-P, (g) CNT@NiFe-Al_2O_3-C-P, and (h) CNT@NiFeAl-C-P.

mass loss regions with higher initiation temperatures (Fig. 3(e-h)), except for CNT@NiFe-Al_2O_3-C-P, where mass loss shifts to higher temperatures, possibly due to metallic particle removal [34]. CNTs from wet impregnation-derived catalysts are more prone to oxidation, showing lower initiation temperatures (400–405 °C and 480–520 °C for as-synthesized and purified CNTs, respectively) compared to co-precipitation-derived catalysts (440–460 °C and 530 °C for as-synthesized and purified, respectively). This difference suggests higher amorphous structure formation in wet impregnation-derived catalysts. This behavior is novel in CNT synthesis literature.

3.1.4. Structure, magnetism and surface chemistry of the materials

Fig. 4 illustrates XRD diffractograms of four CVD-catalysts (Ni-Al_2O_3-I, NiFe-Al_2O_3-I, NiFe-Al_2O_3-C, NiFeAl-C). Catalysts synthesized with support (Ni-Al_2O_3-I, NiFe-Al_2O_3-I, NiFe-Al_2O_3-C) exhibit diffraction peaks corresponding to γ-Al_2O_3 (37.3°, 45.6°, 66.1–66.5°, JCPDS card no. 10–0425 [36]). Ni-Al_2O_3-I also shows peaks indicative of Ni_2O_3 (31.8°, JCPDS card no. 14–0481 [37]). Nickel ferrite, $NiFe_2O_4$ (30.5°, 44.0°, 54.0°, 58.0° and 66.1–66.5°, JCPDS card no. 10–0325), is present in both NiFe-Al_2O_3-I and NiFe-Al_2O_3-C, with co-precipitation-derived materials showing more pronounced presence. NiFeAl-C contains iron and nickel aluminate spinel (31.2°, 36.7°, 44.5°, 59.2°, 65.2°, JCPDS cards no. 007–0068 and 73–1961, respectively) [38–40]. Magnetic hysteresis curves (Figure S9) reveal varied saturation magnetization and coercivity among purified CNTs. CNT@Ni-Al_2O_3-I-P exhibits the highest saturation magnetization (4.03 emu g^{-1}), while CNT@NiFe-Al_2O_3-I-P displays the lowest (0.56 emu g^{-1}) along with the lowest ashes content. Coercivity ranges from 0.02 to 0.3 kOe. These results align with literature, indicating lower magnetization saturation and coercivity in CNTs with embedded metal nanoparticles via CVD compared to other methods [41]. Pictures in Figure S10 show minimal magnetism in CVD-catalysts, enhanced upon CNT growth. After purification, magnetic response decreases, particularly in CNT@NiFe-Al_2O_3-I and CNT@NiFe-Al_2O_3-C, consistent with hysteresis curves.

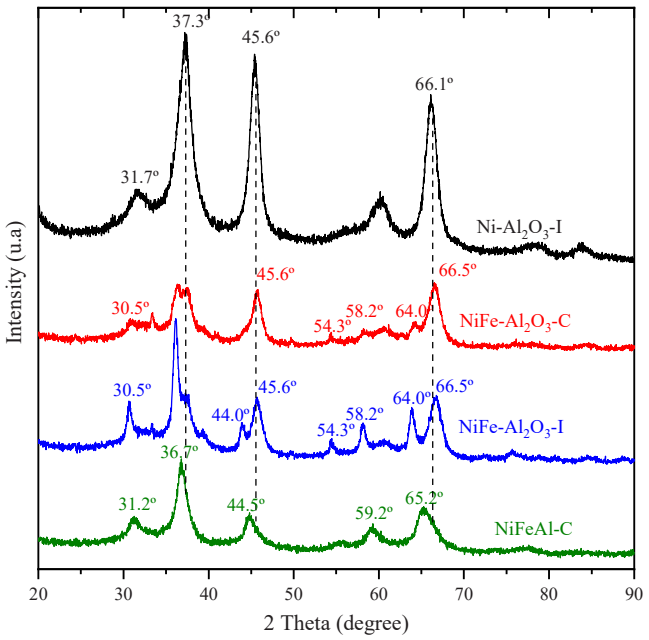

Fig. 4. XRD spectra of each CVD catalyst prepared for the growth of CNTs.

Fig. 5(a) shows FT-IR spectra of CVD-catalysts. Bands below 1000 cm^{-1} are attributed to metal bonds (Fe-O at 569–584 cm^{-1}, Ni-O at 706 cm^{-1}, and Al-O-H at 1065 cm^{-1}) [37,42,43]. The as-synthesized CNTs exhibit other bands in the FT-IR spectra (Fig. 5(b)). The broad band at 3435 cm^{-1} is attributed to O-H bond stretching related to surface moisture [44]. The band at 1635 cm^{-1} corresponds to hydroxyl group bending [44]. A band at 1445 cm^{-1} is characteristic of MWCNTs [45], while the band at 1384 cm^{-1} signifies symmetrical bending of -CH_2 or -CH_3 bonds [44]. Additionally, the 1350 cm^{-1} band indicates C═C stretching [44], and the 872 cm^{-1} band suggests out-of-plane deformation of C-H bonds [44]. Bands in the 1000–500 cm^{-1} range are attributed to the CNT backbone or metal-O-metal bonds from the catalyst, typically absorbed in the 800–200 cm^{-1} range [44]. CNT@NiFe-Al_2O_3-C spectrum reveals bands at 2920 cm^{-1} and 2850 cm^{-1}, indicative of CH_2 group stretching associated with wall surface defects [46]. Similar bands are observed in purified CNTs (Fig. 5(c)), with bands below 1000 cm^{-1} undetectable due to metallic phase removal.

Table S2 presents average contact angles. A clear correlation exists between the synthesis route for CVD catalysts and resulting contact angles. CNT@Ni-Al_2O_3-I-P and CNT@NiFe-Al_2O_3-I-P, grown over wet impregnation-derived catalysts, are more hydrophilic (21.7° and 19.2°, respectively) than the materials resulting from the co-prcipitation method, *i.e.* CNT@NiFe-Al_2O_3-C-P and CNT@NiFeAl-C-P (53.6° and 62.9°, respectively). A study correlating CNT diameters with wettability supports this trend since indicates that CNTs with higher diameters (as those displayed by CNTs grown over wet impregnation-derived CVD catalysts, Figure S4) have lower contact angles [47].

3.2. Application of CNTs as catalysts in wet peroxide oxidation (CWPO)

3.2.1. CWPO with as-synthesized CNTs

Fig. 6 shows the results obtained for the CWPO of PCM as normalized concentration of the model pollutant, H_2O_2 and TOC, considering each as-synthesized CNTs at the operating conditions given in the experimental section. CWPO was also conducted using a commercially-obtained CNT (CNT-C) for comparison purposes. All CNTs displayed catalytic activity (X_{H2O2} > 90 % and X_{PCM} = 63–100 %) compared to a non-catalytic run (X_{H2O2} = 10 % and X_{PCM} = 13 %).

As observed, all CNTs led to the total consumption of H_2O_2 within

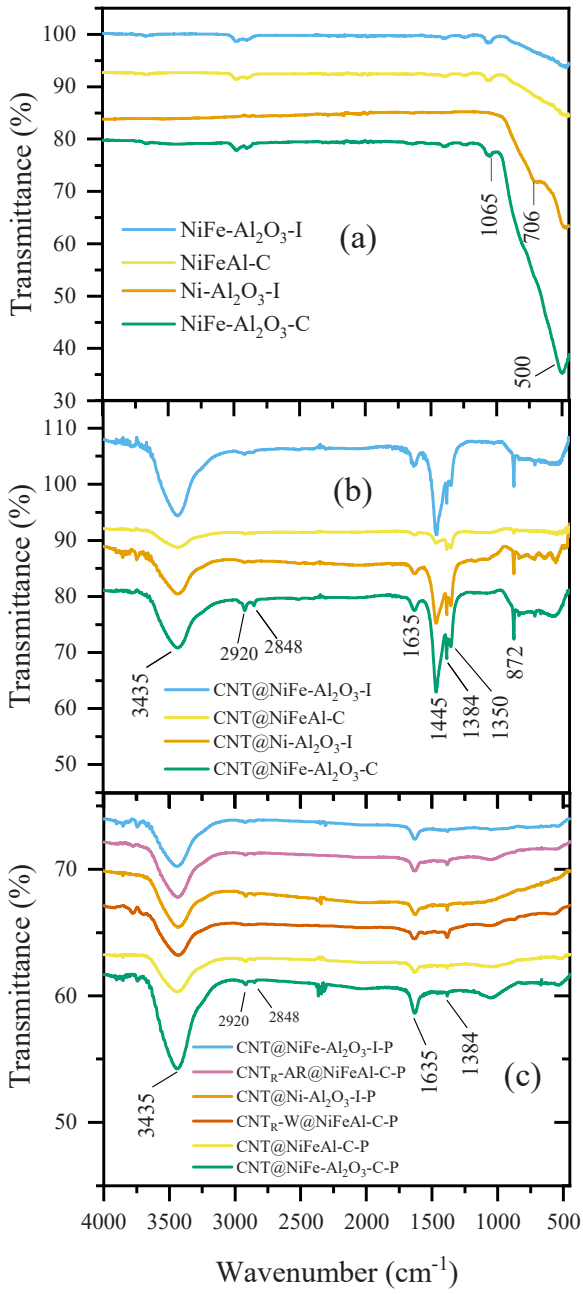

Fig. 5. FT-IR spectra of (a) CVD catalysts, (b) as-synthesized CNTs and (c) purified CNTs.

24 h of reaction (Fig. 6(a)). However, the kinetics of consumption varied greatly amongst the CNTs (initial rates calculated at 30 min are displayed in Table S3). As expected, the CNTs synthesized using CVD-catalysts containing Fe in their structure led to a faster H_2O_2 consumption than the sample obtained in the presence of only Ni (CNT@Ni-Al_2O_3-I). The catalyst that allowed the fastest consumption of H_2O_2 was CNT@NiFeAl-C even though it has a lower content of ashes (12.1 *wt.*%) and of Fe and Ni (2.5 and 0.9 *wt.*%, respectively) compared to the other CNTs (Table 1), with total H_2O_2 consumption being observed within the first 6 h of reaction (Fig. 6(a)). On the other hand, the commercially obtained CNT could completely decompose H_2O_2 within the first 8 h of reaction.

Similarly, most catalysts led to rapid decomposition of PCM, except CNT@Ni-Al_2O_3-I (Fig. 6(b)), resulting in only ~63 % abatement after 24 h of reaction. In contrast, the remaining catalysts could completely decompose PCM within 8 h of reaction. CNT@NiFeAl-C was the catalyst

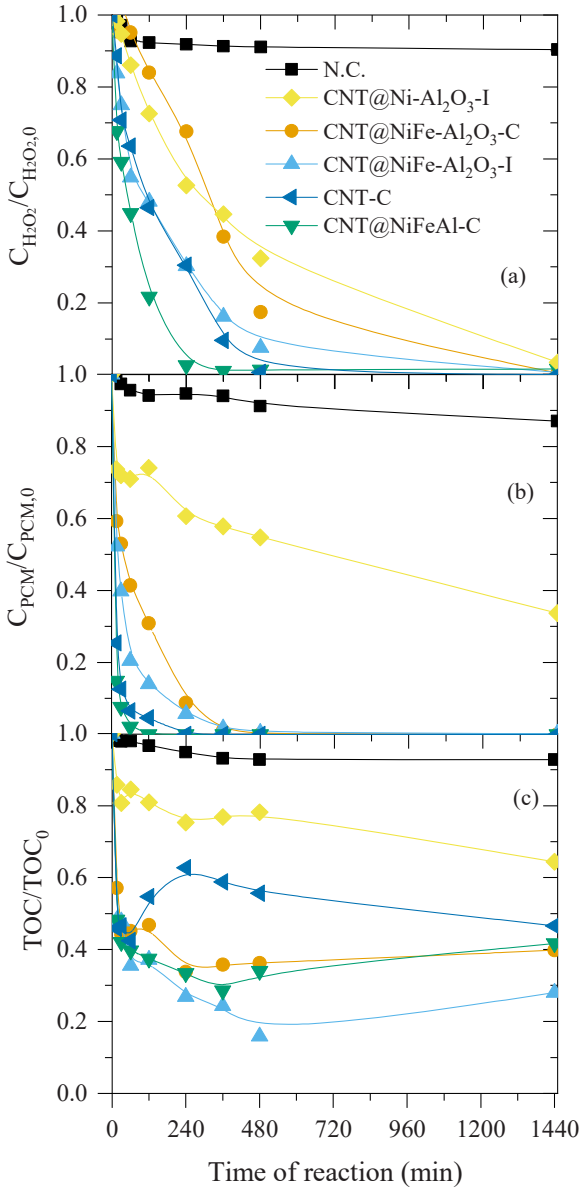

Fig. 6. Normalized concentrations of (a) H_2O_2, (b) PCM and (c) TOC upon time for the originally synthesized CNTs and a commercial CNT sample (CNT-C) (reaction conditions: $[PCM]_0 = 100$ mg L^{-1}, $[H_2O_2]_0 = 474$ mg L^{-1}, 80 °C, $pH_0 = 3.5$, $C_{catalyst} = 2.5$ g L^{-1}). Lines are only intended to guide the eye.

allowing a faster abatement of PCM, achieving 100 % removal in only 2 h of reaction (Fig. 6(b)), and it was also the catalyst promoting fastest consumption of H_2O_2 (Fig. 6(a)). The commercial CNTs led to a complete removal of PCM in 4 h of reaction (Fig. 6(b)).

For both H_2O_2 decomposition and PCM degradation, the results followed the same trend in 2 h of reaction: CNT@NiFeAl-C (X_{H2O2} = 79 % and X_{PCM} = 97 %) > CNT@NiFe-Al_2O_3-I (X_{H2O2} = 69 % and X_{PCM} = 87 %) > CNT@NiFe-Al_2O_3-C (X_{H2O2} = 25 % and X_{PCM} = 69 %) > CNT@Ni-Al_2O_3-I (X_{H2O2} = 27 % and X_{PCM} = 26 %). Presumably, this catalytic activity may be ascribed to both the organic fraction and iron content of each CNT sample, since more active materials (CNT@NiFeAl-C and CNT@NiFe-Al_2O_3-I) show the highest quantity in organic fraction (87.9 *wt.*% and 60.1 *wt.*%, respectively), the second one show the highest content in iron (4.7 *wt.*%), and the catalyst leading to low conversions (CNT@Ni-Al_2O_3-I) has no iron content and a lower organic fraction (50.1 *wt.*%) than the others. The catalytic activity of carbon materials was already explored in the literature, which ascribed electron transfer capabilities as the key to increased catalytic activity towards heterogeneous Fenton reactions [14]. Graphitic carbon phases are recognized to possess better electron transfer properties [48,49], which can explain the enhanced performance of CNT@NiFeAl-C. CNT@NiFeAl-C has *ca.* 1.09 *wt.*% mass loss up to 410 °C, which is smaller than other materials (3.33 *wt.*% for CNT@Ni-Al_2O_3-I, 1.77 *wt.*% for CNT@NiFe-Al_2O_3-I, and 2.79 *wt.*% for CNT@NiFe-Al_2O_3-C), meaning this CNT sample has the lowest amorphous carbon content. Its main oxidation temperature obtained by TGA (702 °C) is also higher than the remaining CNTs (622–692 °C), indicating it to be more graphitic. The total volume of pores was also found to strongly correlate with the conversion of hydrogen peroxide and the PCM (Figure S11(a)). Under the same timeframe (2 h of reaction), the commercial sample resulted in X_{H2O2} = 54 % and X_{PCM} = 95 %.

Regarding the TOC removal (Fig. 6(c)), the catalyst CNT@Ni-Al_2O_3-I was also the worse option, only a ~37 % TOC decrease being verified within 24 h of reaction. Amongst the remaining catalysts, CNT@NiFe-Al_2O_3-I allowed the highest removal (~70 % in 24 h), whereas CNT@NiFe-Al_2O_3-C and CNT@NiFeAl-C led to TOC removals near 60 % in 24 h. TOC removal was also strongly correlated with the total volume of pores (Figure S11(a)). For comparison purposes, CNT-C led to a TOC abatement of 53 % in 24 h. The TOC profile observed for CNT-C sample can be related to the catalyst releasing intermediate from on-site PCM oxidation.

3.2.2. *CWPO with CVD-catalysts before CNT growth*

Fig. 7 shows the results obtained in the CWPO of PCM using the CVD-catalysts (the same ones used to grow CNTs). The decomposition of H_2O_2 ranged between 85 % and 99 % in 24 h (Fig. 7(a)) for all metal substrates, which is comparable to the results obtained considering the derived CNT@CVD-catalysts (Fig. 6(a)), except for Ni-Al_2O_3-I, which resulted in a decomposition of H_2O_2 (10 %) comparable to that obtained in the non-catalytic run (also 10 %). NiFeAl-C led to the fastest consumption of H_2O_2, with over 90 % degradation in about 1 h of reaction. The fastest decomposition observed for this material can be related to the presence of $NiAl_2O_4$ crystalline phase [50], identified by XRD. Despite allowing the decomposition of H_2O_2, the CVD-catalysts were inefficient in removing PCM, with removals obtained in the range of 19–51 % (Fig. 7(b)). The low efficiency of these materials is related to the fast H_2O_2 decomposition observed, which can lead to radical recombination and inefficient degradation of the pollutant [51]. Those removals are much lower compared to the derived CNT@CVD-catalysts (Fig. 6(b)). In fact, in 2 h of reaction using the corresponding CNT@CVD-catalyst, an improvement in PCM removal of 3.9, 4.8, 5.9 and 22 × for CNT@NiFeAl-C, CNT@NiFe-Al_2O_3-I, CNT@NiFe-Al_2O_3-C and CNT@Ni-Al_2O_3-I, respectively, compared to the CVD-catalyst alone, is observed. Similar observations were also made by Zhu *et al.* (2020) when comparing the activity of ferrihydrite and CNT/ferrihydrite on the heterogeneous Fenton degradation of Bisphenol A (BPA) [52]. In the case where CNTs were present, BPA degradation increased 7.1 times due to the ability of the CNTs to enhance the regeneration of Fe^{2+} from Fe^{3+} on the characteristic Fe^{2+}/Fe^{3+} cycles of the Fenton reaction [52], a particular case of CWPO where Fe^{2+}/Fe^{3+} is specifically used as catalyst, Fe^{2+} being more active than Fe^{3+}. The presence of the carbon layer is also expected to increase the adsorption of PCM, thus increasing the local contact between $HO^{\bullet}$ radicals and PCM and the likelihood of reaction between the two species [8,11]. The influence of the carbon content is indisputable, especially when comparing the activity of Ni-Al_2O_3-I and CNT@Ni-Al_2O_3-I. The CVD-catalyst had a similar behavior to the non-catalytic run, meaning it was not an active catalyst in this process. However, the derived CNT did display some activity, achieving a PCM removal of approximately 65 %. Considering that the CVD-catalyst is not active in the CWPO of PCM, the activity observed in the case of CNT@Ni-Al_2O_3-I must come from the carbonaceous layer.

Similar behavior on TOC abatement was observed (Fig. 7(c)). None of the CVD-catalysts were able to replicate or even approximate the

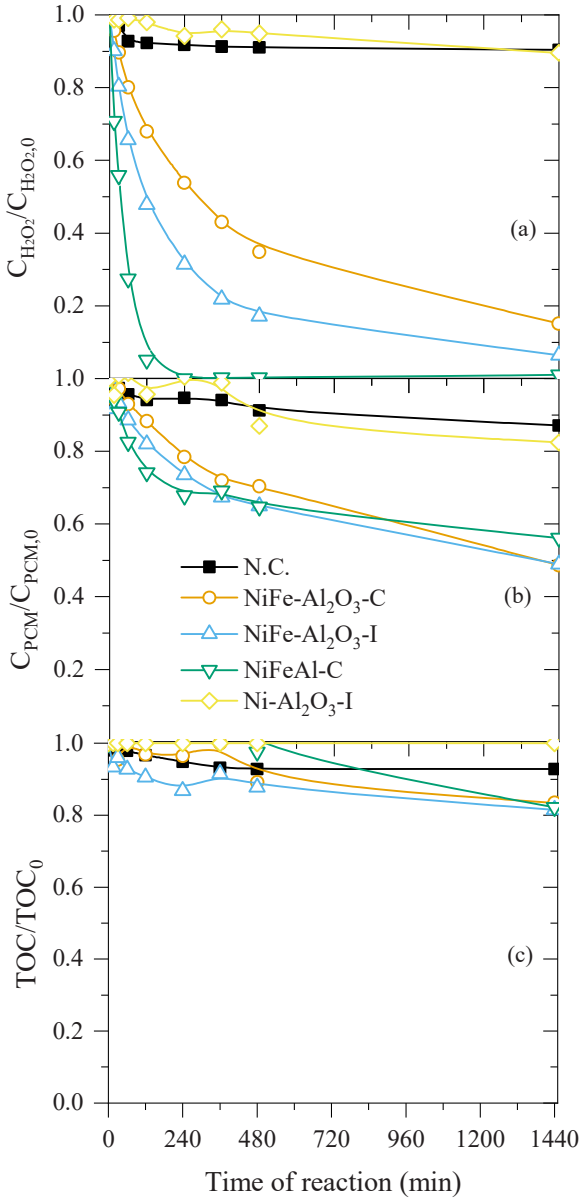

Fig. 7. Normalized concentrations of (a) H_2O_2, (b) PCM, and (c) TOC upon time for the CVD catalysts (reaction conditions: $[PCM]_0 = 100$ mg L^{-1}, $[H_2O_2]_0 = 474$ mg L^{-1}, 80 °C, $pH_0 = 3.5$, $C_{catalyst} = 2.5$ g L^{-1}). Lines are only intended to guide the eye.

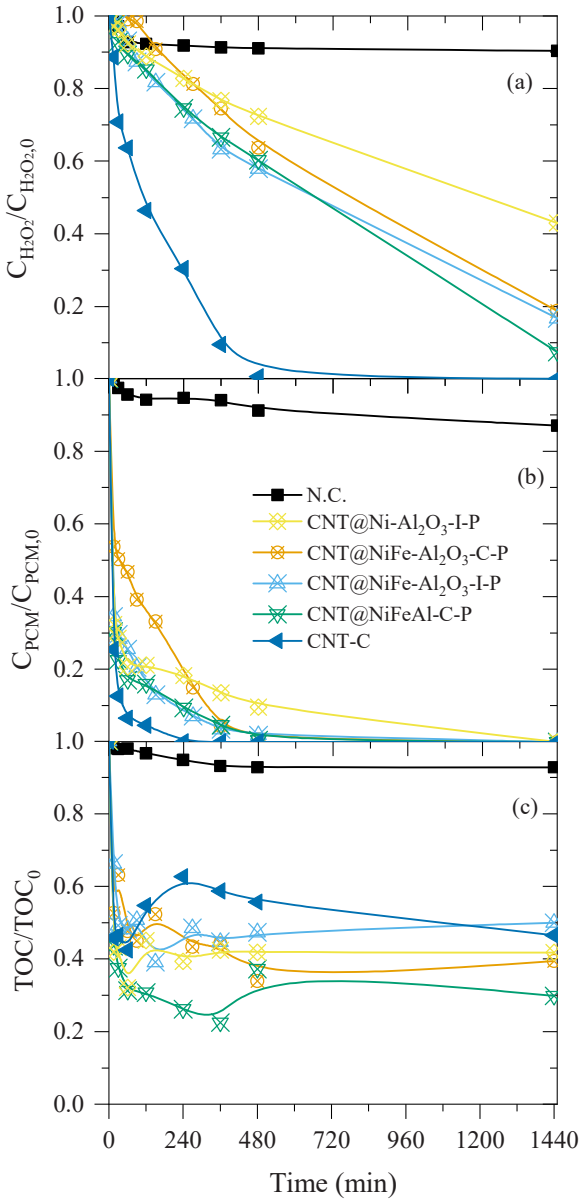

Fig. 8. Normalized concentrations of (a) H_2O_2, (b) PCM, and (c) TOC upon time for the purified CNTs (reaction conditions: $[PCM]_0 = 100$ mg L^{-1}, $[H_2O_2]_0 = 474$ mg L^{-1}, 80 °C, $pH_0 = 3.5$, $C_{catalyst} = 2.5$ g L^{-1}). Lines are only intended to guide the eye.

results obtained using the corresponding CNT@CVD-catalysts (Fig. 6 (c)). In fact, in the presence of Ni-Al_2O_3-I, TOC was barely removed. In 24 h of reaction, Ni-Al_2O_3-I, NiFe-Al_2O_3-I, NiFe-Al_2O_3-C, and NiFeAl-C led to TOC abatements of *ca.* 0, 18, 17 and 18 %, respectively. In the same period, the TOC removal obtained by their derived CNTs was always greater than 37 %.

3.2.3. *CWPO with purified CNTs*

The results regarding the CWPO with the purified CNTs can be found in Fig. 8·H_2O_2 was not completely consumed within 24 h of reaction (Fig. 8(a)), except for CNT-C, and it is also possible to observe that H_2O_2 decomposition was much slower when compared to both the CVD-catalysts (Fig. 7(a)) and the as-synthesized CNTs (Fig. 6(a)). CNT@Ni-Al_2O_3-I-P resulted in the lowest conversion of H_2O_2 (~50 % in 24 h), although having the highest amount of metallic particles after purification (Table 1). However, those metallic particles, comprised of Ni, are not active in the CWPO reaction as previously discussed. CNT@NiFe-Al_2O_3-I-P and CNT@NiFe-Al_2O_3-C-P resulted in ~82 % of H_2O_2 conversion in 24 h, whereas CNT@NiFeAl-C-P resulted in ~93 % of H_2O_2 conversion in the same period.

Concerning the decomposition of PCM, most of the purified CNTs (Fig. 8(b)) behaved similarly to their parent CNTs (Fig. 6(b)), leading to a 100 % decomposition of PCM in 24 h. The only exception is for CNT@Ni-Al_2O_3-I-P, in which its activity was approximately two times higher than its parent CNT (CNT@Ni-Al_2O_3-I). As pointed out above, the activity of CNT@Ni-Al_2O_3-I arises from its carbonaceous layer; thus, removing the metallic particles that are not active in the process seems to increase the access to the active centers of the carbon layer, resulting in an improvement of the removal of PCM. In fact, among the purified CNTs, the amount of ashes was inversely correlated with the PCM removal (Figure S11(b)).

The catalytic activity of the materials in the decomposition of H_2O_2 and removal of PCM follows the pattern: CNT@NiFeAl-C-P (X_{H2O2} = 37 % and X_{PCM} = 95 %) ~ CNT@NiFe-Al_2O_3-I-P (X_{H2O2} = 38 % and

X_{PCM} = 95 %) > CNT@NiFe-Al_2O_3-C-P (X_{H2O2} = 26 % and X_{PCM} = 96 %) > CNT@Ni-Al_2O_3-I-P (X_{H2O2} = 23 % and X_{PCM} = 87 %), similar to what was observed in CWPO when using the as-synthesized CNTs. The purified CNTs resulted in an improvement of PCM removal in the range 2.7–6.6 × higher than the CVD substrate (data from 8 h of reaction).

All purified materials could abate more than 50 % of the TOC (Fig. 8 (c)). CNT@NiFe-Al_2O_3-I-P resulted in a lower abatement than its parent CNT (50 % for purified and 70 % for as-synthesized), whereas CNT@NiFe-Al_2O_3-C-P achieved the same conversion, either as as-synthesized or purified catalyst (~60 % conversion of TOC). On the other hand, CNT@Ni-Al_2O_3-I-P resulted in an increase in TOC removal compared to its parent CNT (61 % *versus* 36 %, respectively). CNT@NiFeAl-C-P also increased TOC abatement compared to CNT@NiFeAl-C: 70 % *versus* 60 %, respectively, in 24 h of reaction. This increment in TOC removal in the presence of CNT@NiFeAl-C-P can be ascribed to the slower decomposition of H_2O_2 when compared to the parent CNT. The contact angle of the samples seems to influence the TOC removal (data at 24 h of reaction): wetness impregnation-derived samples (CA of 19–21°) resulted in lower TOC removals (50–55 %) compared to co-precipitation-derived CNTs (CA of 53–63° and TOC removals of 60–70 %), with CNT@NiFeAl-C-P (CA of 63°) resulting in the highest TOC removal (70 %).

Other papers investigating PCM abatement by advanced oxidation process reported 50 % TOC abatement using pillared clays [10], 63 % TOC abatement using multi-core shell iron oxide nanoparticles [13], 60–75 % for photopolymer-derived carbon materials [14] for Fenton-like process (in 24 h), and 50–61 % for US-assisted electro-n-Fenton using hematite nanoparticles in 1 h [53]. However, in most cases, the materials are metal-based, which can still lead to efficiency loss after repeated cycles due to iron leaching or active phase inactivation.

3.2.4. *Comparison of initial reaction rate among the catalytic materials*

The initial reaction rate for the removal of PCM was also compared between all materials (calculated as Δn/Δt at 30 min of reaction time) and the results are given in Table S3. As can be observed, among the same class of material (CVD-catalyst, as-synthesized or purified CNT), the materials derived from NiFeAl-C always show the highest initial reaction rate. This is very evident among the as-synthesized CNTs, where the initial reaction rate displayed by CNT@NiFeAl-C is at least 1.5 times faster than those of the remaining materials. The commercial sample (CNT-C) also shows a high initial reaction rate, despite performing poorer in other measured parameters (such as lower TOC removal and lower efficiency of H_2O_2 consumption, as previously discussed). It should also be noted that for some of the CVD-catalysts (Ni-Al_2O_3-I and NiFe-Al_2O_3-C) the initial rate displayed is virtually the same as that of the non-catalytic run.

The same trend in the abatement of PCM and TOC was observed in removing total phenolic compounds (TP) and aromatic compounds (ARM) among all the catalysts studied in previous sections (Figure S12). CVD-catalysts resulted in a removal of TP and ARM of 5–45 % and 1–43 %, respectively (Figure S12 (a)). The as-synthesized CNTs (Figure S12 (b)) and purified CNTs (Figure S12 (c)) greatly surpassed the activity of the CVD-catalysts, leading to abatements in the range of 63–100 % and 65–100 % for TP and ARM, respectively. Moreover, the TOC that is not resulting from PCM (subtracting the contribution of the theoretical TOC attributed to PCM) is represented in Figure S13, which increased and thus suggested the formation of some refractory reaction by-products.

Fig. 9 presents the efficiency of consumption of H_2O_2 in 24 h of reaction (η_{H2O2}) calculated according to Eq. S1. This efficiency was approximately 20 % for the CVD-catalysts containing Fe and *ca.* 0 % for the CVD-catalyst based only on Ni. In addition, most of the purified CNTs resulted in more efficient consumption of H_2O_2 when compared to the as-synthesized CNTs, and especially when compared to the CVD-catalysts. The only exception is for CNT@NiFe-Al_2O_3-I-P, which

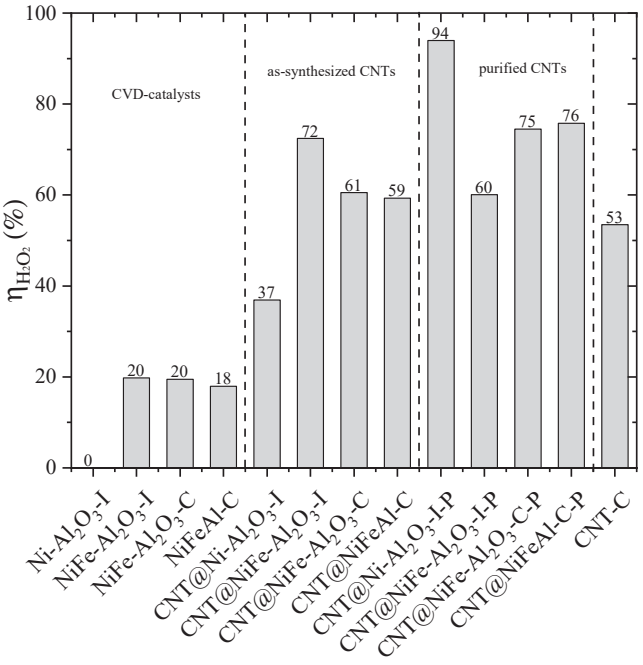

Fig. 9. Efficiency of H_2O_2 consumption after 24 h of reaction (CWPO of PCM) (reaction conditions: $[PCM]_0$ = 100 mg L^{-1}, $[H_2O_2]_0$ = 474 mg L^{-1}, 80 °C, pH_0 = 3.5, $C_{catalyst}$ = 2.5 g L^{-1}).

resulted in lower efficiency than CNT@NiFe-Al_2O_3-I (60 and 72 %, respectively). Furthermore, most of the CNTs synthesized in this work resulted in higher efficiency of H_2O_2 compared to the commercially available CNT-C (53 %). The highest efficiency (76 %) was observed with CNT@NiFeAl-C-P, followed closely by CNT@NiFe-Al_2O_3-C-P (75 %). CNT@Ni-Al_2O_3-I-P resulted in an efficiency of *ca.* 94 %. However, this result may be attributed to the adsorption behavior of this CNT sample, as will be shown in the following section. Thus, this value must be carefully interpreted. The results reported here agree with previously reported efficiencies for abatement of micropollutants in the presence of CNTs [11,15,22,54].

Figure S14 compares the contributions of CWPO (8 h of reaction) and adsorption (24 h of contact time) in removing PCM for all catalysts. In general, CVD-catalysts (Figure S14 (a)) do not adsorb PCM, except NiFeAl-C with an adsorption of *ca.* 25 %. For the CNTs, the adsorption contribution increases after purification (Figure S14 (b) and (c), respectively), which may indicate that the metal particles were blocking the active centers of the CNTs. In some cases, such as for CNT@Ni-Al_2O_3-I, CNT@Ni-Al_2O_3-I-P, CNT@NiFe-Al_2O_3-I-P and CNT@NiFe-Al_2O_3-C-P, the adsorption effect is relevant, with an emphasis in CNT@Ni-Al_2O_3-I-P where 80 % of PCM is removed by adsorption only. In comparison, CWPO resulted in a removal of 90 %. This high contribution of adsorption in CNT@Ni-Al_2O_3-I-P may explain the odd behavior reported regarding the efficiency of H_2O_2 consumption. Similar results were obtained with CNT-C, where the adsorption contribution is *ca.* 75 %. Considering the high adsorption capacity shown by the CNTs, desorption runs were carried out with CNTs recovered from CWPO reactions to ensure that the removal of PCM is ascribed to oxidation rather than adsorption. With the exception of CNT@Ni-Al_2O_3-I-P, no PCM desorbed from the catalyst surface or other possible degradation products were identified, indicating that all PCM adsorbed in the catalyst surface was oxidized and desorbed. For the desorption runs with CNT@Ni-Al_2O_3-I-P, PCM was identified in a concentration of 5 mg_{PCM} g_{cat}^{-1}.

CNTs bear two roles in the process. The first role is as a catalyst for the decomposition of hydrogen peroxide. The mechanism of hydrogen peroxide decomposition in pure carbon materials is expected to occur in both reducing and oxidizing active sites (yielding hydroxyl and

hydroperoxyl radicals, respectively) on the carbon surface, as thoroughly explained elsewhere [55]. For the CNTs with metallic particles (as-synthesized CNTs), the metallic particles likely play a role in decomposing H_2O_2 through a typical Fenton/Fenton-like mechanism [56], reflecting in an accelerated H_2O_2 decomposition as seen in Fig. 6. The second role of the CNTs is as an adsorbent. High adsorptive interactions between the pollutant and catalyst phase result in an increased pollutant concentration near the active sites where active radicals ($HO^{\bullet}$) are formed, increasing the likelihood of contact between these radicals and PCM molecules, eventually promoting the oxidation of PCM and avoiding side reactions between H_2O_2 and $HO^{\bullet}$ [8,57].

3.2.5. Leaching of metallic species

Fig. 10 displays Ni and Fe concentrations in the aqueous phase of reaction media after CWPO runs, which was monitored to study the metal leaching from catalysts (CVD-catalysts, as-synthesized CNTs and purified CNTs). Higher concentrations of Ni and Fe in the treated water were found for the reactions conducted in the presence of the CVD-catalysts, followed by the as-synthesized CNTs. Lower concentrations were found for the purified samples.

In the presence of the CVD-catalysts, significant leaching was verified, especially in the case of NiFeAl-C, with ~1.5 mg L^{-1} of leached Fe, indicating that there might be some contribution of homogeneous Fenton reaction in the case of this catalyst, and *ca.* 6.1 mg L^{-1} of Ni with Ni-Al_2O_3-I. Nevertheless, the percentual of leaching was not so high (<5 % for Ni and <0.6 % for Fe) since CVD-catalysts have a high content of these metals.

The materials derived from Ni-Al_2O_3-I presented poor stability even after the growth and purification of the CNTs. CNT@Ni-Al_2O_3-I resulted in *ca.* 5.5 mg L^{-1} of Ni in the solution, representing a 13 % leaching of its Ni content, whereas CNT@Ni-Al_2O_3-I-P resulted in *ca.* 4.8 mg L^{-1} of Ni (*ca.* 2 % leaching of its Ni content). Although there is some improvement in terms of stability, the results still surpass those allowed for the content of Ni in drinking water [58].

For the remaining materials, the contents of Ni and Fe in the treated water greatly decreased. The concentration of Fe in this water never surpasses 0.4 and 0.2 mg L^{-1} for as-synthesized and purified CNTs, whereas 0.7 and 0.3 mg L^{-1} of Ni were determined for as-synthesized and purified CNTs, respectively. The metal leaching was reduced when applying purified CNTs (0–88 % for Fe and 60–99 % for Ni) compared to the as-synthesized CNTs. However, the difference in metal leaching between CVD-catalysts and as-synthesized CNTs or purified CNTs depended greatly on the pairs being compared. Among all the purified catalysts, the lowest Ni and Fe leaching was observed for CNT@NiFeAl-C-P and CNT@NiFe-Al_2O_3-C-P. In the case of the first, the concentrations of Ni and Fe in water were lower (0.003 and 0.08 mg L^{-1}, respectively) compared to the latter (0.20 and 0.13 mg L^{-1}, respectively). In terms of stability, CNT@NiFe-Al_2O_3-C-P resulted in a lower percentual leaching of Fe (0.31 % vs 0.64 % for CNT@NiFeAl-C-P) and a higher percentual leaching of Ni (1.33 % vs 0.02 % for CNT@NiFeAl-C-P). The only material that resulted in a lower leaching than the guidelines suggested by the World Health Organization (WHO/SDE/WSH/07.08/55) of 0.07 mg L^{-1} of Ni in drinking waters [58] is CNT@NiFeAl-C-P.

As CNT@NiFeAl-C-P resulted in the lowest concentration of metallic species in the effluent with a suitable stability, efficient H_2O_2 consumption, ability to completely decompose PCM and to remove 70 % of TOC, further studies were carried out with materials based on CNT@NiFeAl-C-P.

3.2.6. Evaluating the role of acid washing in CWPO

The influence of the acid washing on the rate of CWPO was evaluated by washing CNT@NiFeAl-C with distinct concentrations of H_2SO_4 (10 and 30 %), leading to CNT@NiFeAl-C-10 and CNT@NiFeAl-C-30, respectively. The results obtained for the CWPO reactions are given in Fig. 11. As observed (Fig. 11 (a)), CNT@NiFeAl-C-10 results in a slightly worse performance when compared to the other samples; however, it reaches a removal of PCM above 90 % in 2 h of reaction, a result also observed for the other samples, so it does not appear to exist any correlation between the concentration of acid and the removal of PCM. However, when it comes down to the consumption of H_2O_2 (Fig. 11 (a)), a clear difference between the as-synthesized material and the purified ones is observed. In the case of CNT@NiFeAl-C, its activity is very likely ascribed to the content of Fe in its structure, as previously discussed. For CNT@NiFeAl-C-P, on the other hand, the content of Fe is similar to the remaining acid-washed CNTs, which may indicate a higher incorporation of oxygen and sulfur-containing groups on its surface when compared to the other acid-washed CNTs. Both oxygen [59] and sulfur [60] surface groups have been linked to alterations in the decomposition of H_2O_2 during AOPs. Nevertheless, all materials resulted in complete

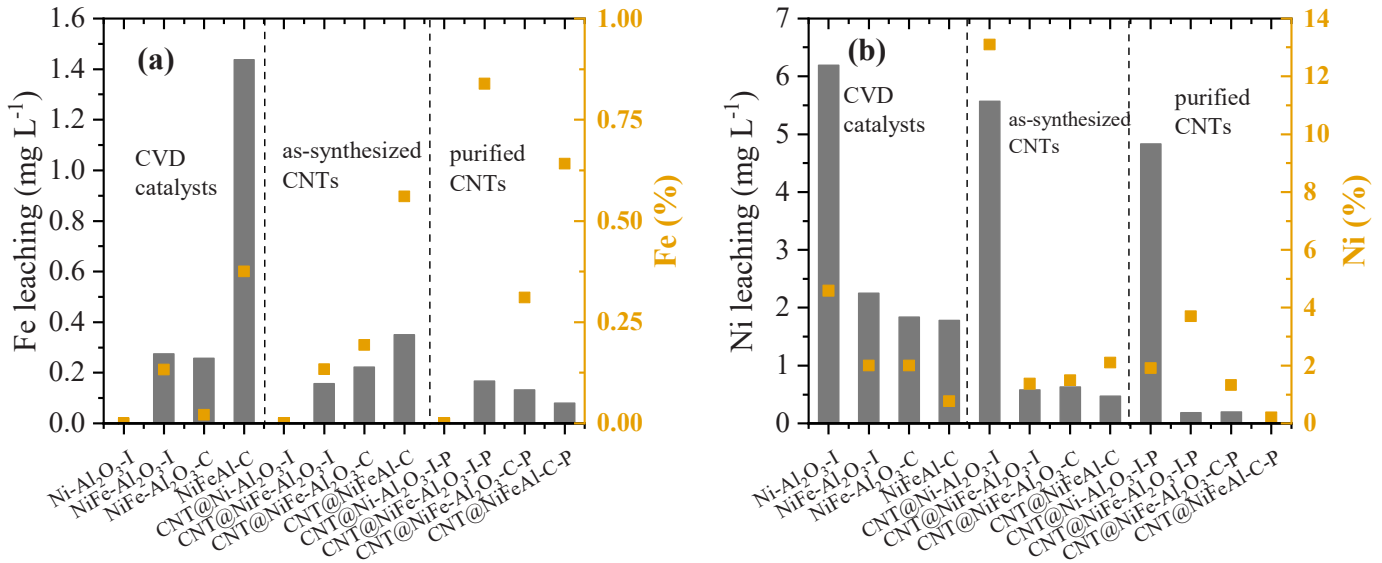

Fig. 10. Metal leaching after 24 h of reaction (CWPO of PCM) (left Y-axis (black): concentration of metal leaching in the reaction effluent and right Y-axis (yellow): percentual of metal leaching according to the metal content of the material). (Reaction conditions: $[PCM]_0 = 100$ mg L^{-1}, $[H_2O_2]_0 = 474$ mg L^{-1}, 80 °C, $pH_0 = 3.5$, $C_{catalyst} = 2.5$ g L^{-1}).

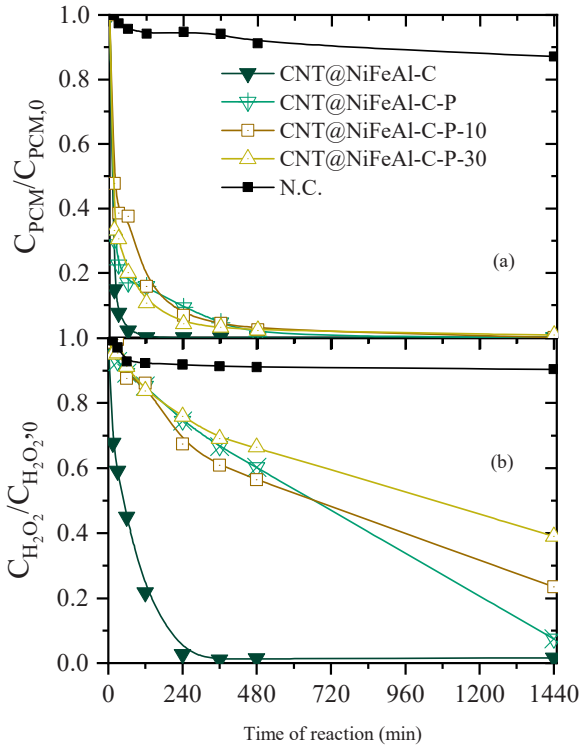

Fig. 11. Normalized concentrations of (a) PCM and (b) H_2O_2 upon time for the CNTs derived from CNT@NiFeAl-C (reaction conditions: $[PCM]_0 = 100$ mg L^{-1}, $[H_2O_2]_0 = 474$ mg L^{-1}, 80 °C, $pH_0 = 3.5$, $C_{catalyst} = 2.5$ g L^{-1}). Lines are only intended to guide the eye.

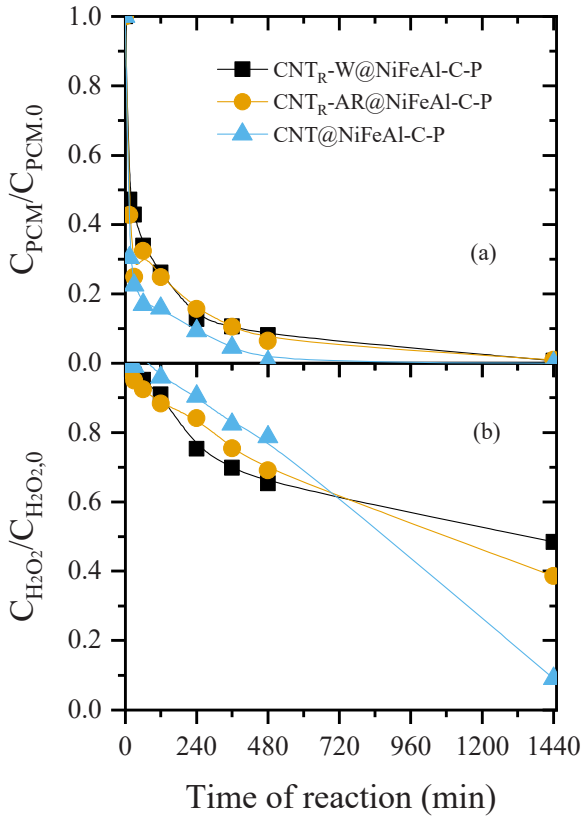

Fig. 12. Normalized concentrations of (a) PCM and (b) H_2O_2 upon time for the CNTs obtained from real PSW (reaction conditions: $[PCM]_0 = 100$ mg L^{-1}, $[H_2O_2]_0 = 474$ mg L^{-1}, 80 °C, $pH_0 = 3.5$, $C_{catalyst} = 2.5$ g L^{-1}). Lines are only intended to guide the eye.

PCM removal (Fig. 11 (a)) and complete removal of TP and ARM (Figure S12 (d)) in 24 h of reaction. Adsorption contribution was also evaluated for these materials (Figure S14 (d)). Regardless of the acid concentration used, the adsorption contribution varied in the range *ca.* 50–65 % in 24 h of reaction.

Finally, the leaching of Fe was lower for acid-washed CNTs for concentrations higher than 30 %, with a reduction of Fe leaching of approximately 47 % and 77 % when acid concentrations of 30 % or 50 % were used, compared to an acid concentration of 10 % where no evident effect over leaching was seen (Figure S15 (a)). Ni leaching was reduced by over 90 % regardless of the acid concentration. For both metals, there is an evident correlation between acid concentration and leaching of metallic species, where increasing acid concentration results in a decreased leaching, with R^2 of 0.96 and 0.88 for Fe and Ni, respectively (Figure S15 (b) and (c)). Therefore, 30 % concentration of H_2SO_4 seems suitable to remove metallic particles and stabilize the samples.

3.3. CNTs obtained from LDPE waste: proof-of-concept

The materials obtained from LDPE waste were applied in the removal of PCM by CWPO as a proof-of-concept and the results are presented in Fig. 12. As it can be observed, both CNT_R-W@NiFeAl-C-P and CNT_R-AR@NiFeAl-C-P behaved similarly in terms of PCM abatement, although their activity was slightly lower when compared to CNT@NiFeAl-C-P. While CNT@NiFeAl-C-P resulted in a PCM removal of 100 % in 8 h of reaction, under the same timeframe, the samples derived from real PSW resulted in 90 %, requiring the full 24 h of reaction for complete PCM degradation.

In terms of H_2O_2 decomposition, the behavior of the samples derived from PSW resulted in a slightly faster decomposition of H_2O_2 in the first 8 h of reaction, but by the end of reaction, CNT@NiFeAl-C-P led to over 90 % of H_2O_2 consumption, whereas CNT_R-W@NiFeAl-C-P and CNT_R-AR@NiFeAl-C-P resulted in 50 and 60 % decomposition, respectively. Adsorption effect was also assessed for those materials, with a contribution of 50 and 65 % for CNT_R-W@NiFeAl-C-P and CNT_R-AR@NiFeAl-C-P, respectively (Figure S16 (a)). TOC, ARM and TP removals were similar to those observed with CNT@NiFeAl-C-P, with ARM and TP removals over 95 % and TOC at around 65–71 % (Figure S16 (b)), and leaching of metallic species was very low (<0.05 mg L^{-1} for Ni and 0.10–0.12 mg L^{-1} for Fe). Differently to the observed with the pure sample (CNT@NiFeAl-C-P), CNT_R-W@NiFeAl-C-P and CNT_R-AR@NiFeAl-C-P did result in some adsorbed PCM remaining in the catalyst during CWPO reactions: desorption studies revealed an accumulation of 0.5 and 0.6 mg_{PCM} $g_{catalyst}^{-1}$ for CNT_R-W@NiFeAl-C-P and CNT_R-AR@NiFeAl-C-P, respectively. Other intermediates adsorbed in the catalyst were also identified: *p*-benzoquinone with an accumulation of 0.1 mg $g_{catalyst}^{-1}$ regardless of the catalyst. CNT_R-AR@NiFeAl-C-P was recovered from the reaction medium and reutilized in subsequent runs. The results are displayed in Figure S17. As observed, the activity of CNT_R-AR@NiFeAl-C-P remains largely the same, both for PCM removal (89–94 % in 6 h of reaction) and H_2O_2 conversion (57–67 % in 24 h of reaction).

Despite some differences in activity between CNTs obtained from pure polymer versus CNTs from LDPE from real PSW samples, the CNTs obtained from PSW as carbon source are also suitable catalysts for CWPO applications. Further investigations into this type of applications are needed, as the relationship between PSW composition, the characteristics of CNTs and their catalytic activity must be better correlated for deliberated designs of catalyst particles. As far as we are aware, only two other works report the catalytic activity of CNTs derived from actual PSW for AOPs [61,62].

4. Conclusions

In this work, we demonstrate the successful preparation of carbon nanotubes from low-density polyethylene, considering distinct substrates for the growth of the nanostructured carbon materials, obtaining yields in the range of 16–33 wt%. To the best of our knowledge, no other study presents a detailed characterization of CNTs and a fair comparison between purified and non-purified materials. It is evident that both the substrate and the route for their obtention influence the CNT sample synthesized. Co-precipitation-derived CNTs resulted in curly CNTs, while wet-impregnation resulted in CNTs with straight walls.

The CNTs were applied in the CWPO of a model pollutant – PCM – and both as-synthesized and purified CNTs were active in the process (X_{PCM} = 100 %, X_{H2O2} > 50 % in 24 h). Special attention should be given to the obvious role of the carbon layer in the decomposition of H_2O_2 and abatement of PCM and TOC, as the activity shown by CNTs surpassed the activity of the substrates by at least 3.8 times, reaching an improvement of up to 22 times, depending on the pair being compared. It was also demonstrated that the purified CNTs result in higher activity (X_{PCM} = 100 %, X_{H2O2} > 50 % in 24 h) compared to pure CVD substrates (X_{PCM} < 50 %, X_{H2O2} > 80 % in 24 h) and, in some cases, its activity surpasses the CNT bearing a metal phase, especially when it comes down to the efficiency of H_2O_2 consumption. Distinct concentrations of sulfuric acid (10–50 %) allowed removing metallic particles, and concentrations of acid above 30 % already result in less leaching of metallic species and slower consumption of H_2O_2. In turn, the efficiency of consumption of the oxidant increases.

Finally, the activity of CNTs derived from real PSW samples was also assessed; despite some differences compared to the pure samples (X_{PCM} = 98 %, X_{H2O2} = 60 % for waste LDPE *versus* X_{PCM} = 100 %, X_{H2O2} = 90 % for pure LDPE, 24 h), suitable activities were observed with real samples, which were maintained for 3 cycles with differences lower than 5 %, indicating the feasibility of the system.

Author statement

During the preparation of this work the authors used ChatGPT in order to improve the readability/English language. After using this tool/service, the authors reviewed and edited the content as needed and take full responsibility for the content of the publication.

CRediT authorship contribution statement

Fernanda Fontana Roman: Writing – original draft, Visualization, Validation, Investigation, Formal analysis, Conceptualization. **Helder T. Gomes:** Writing – review & editing, Supervision, Project administration, Funding acquisition. **Adriano S. Silva:** Writing – original draft, Investigation. **Jose L. Diaz de Tuesta:** Writing – review & editing, Supervision, Project administration, Methodology, Funding acquisition, Conceptualization. **Arthur P. Baldo:** Writing – review & editing, Investigation. **Paulo Praça:** Writing – review & editing, Resources, Project administration. **Adrián M. T. Silva:** Writing – review & editing, Supervision. **Joaquim Faria:** Writing – review & editing, Supervision. **Manuel Bañobre-López:** Writing – review & editing, Investigation. **Jessica P. M. Lopes:** Investigation. **Giane Gonçalves:** Writing – review & editing, Supervision. **Ana Pereira:** Writing – review & editing, Supervision.

Declaration of Competing Interest

The authors declare that they have no known competing financial interests or personal relationships that could have appeared to influence the work reported in this paper

Acknowledgments

This work was financially supported by project "PLASTIC_TO_FUEL&MAT – Upcycling Waste Plastics into Fuel and Carbon Nanomaterials" (PTDC/EQU-EQU/31439/2017), and by national funds through FCT/MCTES (PIDDAC): CeDRI, UIDB/05757/2020 (DOI: 10.54499/UIDB/05757/2020) and UIDP/05757/2020 (DOI: 10.54499/UIDB/05757/2020); CIMO, UIDB/00690/2020 (DOI: 10.54499/UIDB/00690/2020) and UIDP/00690/2020 (DOI: 10.54499/UIDP/00690/2020); SusTEC, LA/P/0007/2020 (DOI: 10.54499/LA/P/0007/2020); LSRE-LCM, UIDB/50020/2020 (DOI: 10.54499/UIDB/50020/2020) and UIDP/50020/2020 (DOI: 10.54499/UIDP/50020/2020); ALiCE, LA/P/0045/2020 (DOI: 10.54499/LA/P/0045/2020); and PTDC/CTA-AMB/3489/2021 - RECY-SMARTE (DOI 10.54499/PTDC/CTA-AMB/3489/2021). Fernanda F. Roman acknowledges the national funding by FCT and the European Social Fund, FSE, through the individual research grant SFRH/BD/143224/2019. Adriano S. Silva was supported by the doctoral Grant SFRH/BD/151346/2021 financed by FCT with funds from NORTE2020, under MIT Portugal Program. Jose L. Diaz De Tuesta acknowledges the financial support through the program of *Atracción al Talento* of *Comunidad de Madrid* (Spain) for the individual research grant 2022-T1/AMB-23946. The authors are also grateful for the finantial support provided by Sociedade Ponto Verde for the project "*Estudo técnico-económico para a valorização de resíduos de embalagens plásticas na produção de nanotubos de carbono*".

Appendix A. Supporting information

Supplementary data associated with this article can be found in the online version at doi:10.1016/j.jece.2024.115206.

Data availability

Data will be made available on request.

References

[1] PlasticsEurope, Plastics - the facts 2021, 2021.
[2] W.W.Y. Lau, Y. Shiran, R.M. Bailey, E. Cook, M.R. Stuchtey, J. Koskella, C.A. Velis, L. Godfrey, J. Boucher, M.B. Murphy, R.C. Thompson, E. Jankowska, A. Castillo Castillo, T.D. Pilditch, B. Dixon, L. Koerselman, E. Kosior, E. Favoino, J. Gutberlet, S. Baulch, M.E. Atreya, D. Fischer, K.K. He, M.M. Petit, U.R. Sumaila, E. Neil, M. V. Bernhofen, K. Lawrence, J.E. Palardy, Evaluating scenarios toward zero plastic pollution, Science (2020) 1455–1461, https://doi.org/10.1126/science.aba9475.
[3] N. Singh, D. Hui, R. Singh, I.P.S. Ahuja, L. Feo, F. Fraternali, Recycling of plastic solid waste: a state of art review and future applications, Compos. Part B Eng. 115 (2017) 409–422, https://doi.org/10.1016/j.compositesb.2016.09.013.
[4] C. Zhuo, Y.A. Levendis, Upcycling waste plastics into carbon nanomaterials: a review, J. Appl. Polym. Sci. 131 (4) (2014) 39931, https://doi.org/10.1002/app.39931.
[5] Plastic upcycling, Nature Catalysis 2(11) (2019) 945-946. https://doi.org/10.1038/s41929-019-0391-7..
[6] R. Kumar, R.K. Singh, D.P. Singh, Natural and waste hydrocarbon precursors for the synthesis of carbon based nanomaterials: graphene and CNTs, Renew. Sustain. Energy Rev. 58 (2016) 976–1006, https://doi.org/10.1016/j.rser.2015.12.120.
[7] N. Hiremath, G. Bhat, High-performance carbon nanofibers and nanotubes, Struct. Prop. High. Perform. Fibers (2017) 79–109, https://doi.org/10.1016/b978-0-08-100550-7.00004-8.
[8] R.S. Ribeiro, A.M.T. Silva, J.L. Figueiredo, J.L. Faria, H.T. Gomes, Catalytic wet peroxide oxidation: a route towards the application of hybrid magnetic carbon nanocomposites for the degradation of organic pollutants. A review, Appl. Catal. B Environ. 187 (2016) 428–460, https://doi.org/10.1016/j.apcatb.2016.01.033.
[9] R.S. Ribeiro, A.M.T. Silva, P.B. Tavares, J.L. Figueiredo, J.L. Faria, H.T. Gomes, Hybrid magnetic graphitic nanocomposites for catalytic wet peroxide oxidation applications, Catal. Today 280 (2017) 184–191, https://doi.org/10.1016/j.cattod.2016.04.040.
[10] A. Santos Silva, M. Seitovna Kalmakhanova, B. Kabykenovna Massalimova, J. G. Sgorlon, D.D.T. Jose Luis, H.T. Gomes, Wet peroxide oxidation of paracetamol using acid activated and Fe/Co-pillared clay catalysts prepared from natural clays, Catalysts 9 (9) (2019) 705, https://doi.org/10.3390/catal9090705.
[11] J.L. Diaz de Tuesta, A.S. Silva, F.F. Roman, L.F. Sanches, F.A. da Silva, A.I. Pereira, A.M.T. Silva, J.L. Faria, H.T. Gomes, Polyolefin-derived carbon nanotubes as magnetic catalysts for wet peroxide oxidation of paracetamol in aqueous solutions, Catal. Today 419 (2023) 114162, https://doi.org/10.1016/j.cattod.2023.114162.

[12] F.F. Roman, J.L. Diaz de Tuesta, F.K.K. Sanches, A.S. Silva, P. Marin, B.F. Machado, P. Serp, M. Pedrosa, A.M.T. Silva, J.L. Faria, H.T. Gomes, Selective denitrification of simulated oily wastewater by oxidation using Janus-structured carbon nanotubes, Catal. Today (2023) 114001, https://doi.org/10.1016/j.cattod.2023.01.008.
[13] A.S. Silva, F.F. Roman, A.V. Dias, J.L. Diaz de Tuesta, A. Narcizo, A.P.F. da Silva, I. Çaha, F.L. Deepak, M. Bañobre-López, A.M.C. Ferrari, H.T. Gomes, Hybrid multi-core shell magnetic nanoparticles for wet peroxide oxidation of paracetamol: application in synthetic and real matrices, J. Environ. Chem. Eng. 11 (5) (2023) 110806, https://doi.org/10.1016/j.jece.2023.110806.
[14] A.S. Silva, J.L. Diaz de Tuesta, A. Henrique, F.F. Roman, D. Omralinov, H. Steldinger, J. Gläsel, B.J.M. Etzold, J.A.C. Silva, A.M.T. Silva, A.I. Pereira, H. T. Gomes, 3D printed photopolymer derived carbon catalysts for enhanced wet peroxide oxidation, Chem. Eng. J. 499 (2024), https://doi.org/10.1016/j.cej.2024.156574.
[15] R.S. Ribeiro, O. Vieira, R. Fernandes, F.F. Roman, J.L. Diaz de Tuesta, A.M.T. Silva, H.T. Gomes, Synthesis of low-density polyethylene derived carbon nanotubes for activation of persulfate and degradation of water organic micropollutants in continuous mode, J. Environ. Manag. 308 (2022) 114622, https://doi.org/10.1016/j.jenvman.2022.114622.
[16] S. Hussain, E. Aneggi, D. Goi, Catalytic activity of metals in heterogeneous Fenton-like oxidation of wastewater contaminants: a review, Environ. Chem. Lett. 19 (3) (2021) 2405–2424, https://doi.org/10.1007/s10311-021-01185-z.
[17] M. Zhang, K.P. Annamalai, L. Liu, T. Chen, J. Gao, Y. Tao, Multiwalled carbon nanotube-supported CuCo2S4 as a heterogeneous Fenton-like catalyst with enhanced performance, RSC Adv. 7 (34) (2017) 20724–20731, https://doi.org/10.1039/c7ra01269a.
[18] W. Li, Q. Zhu, X. Yin, Z. Gao, K. Wei, S. Liu, X. Zhang, H. Chen, Y. Zhang, W. Han, Enhanced heterogeneous Fenton catalysis by carbon nanotube-loaded Mn doped FeS2 catalysts for pollutant degradation: Co-enhancement effect of Fe-S-Mn and Fe-S-C linkages, Sep. Purif. Technol. 335 (2024), https://doi.org/10.1016/j.seppur.2023.126150.
[19] H.N. Phong Vo, G.K. Le, T.M. Hong Nguyen, X.T. Bui, K.H. Nguyen, E.R. Rene, T.D. H. Vo, N.D. Thanh Cao, R. Mohan, Acetaminophen micropollutant: historical and current occurrences, toxicity, removal strategies and transformation pathways in different environments, Chemosphere 236 (2019) 124391, https://doi.org/10.1016/j.chemosphere.2019.124391.
[20] C. Wu, M.A. Nahil, N. Miskolczi, J. Huang, P.T. Williams, Production and application of carbon nanotubes, as a co-product of hydrogen from the pyrolysis-catalytic reforming of waste plastic, Process Saf. Environ. Prot. 103 (2016) 107–114, https://doi.org/10.1016/j.psep.2016.07.001.
[21] M.A. Jayan, S.S. Dawn, G.G.V. Kumar, Nano-structured manganese promoted ferrous catalyst synthesized by incipient wetness impregnation method: synthesis and characterization, Mater. Lett. 240 (2019) 55–58, https://doi.org/10.1016/j.matlet.2018.12.115.
[22] F.F. Roman, L. De Grande Piccinin, A. Santos Silva, J.L. Diaz de Tuesta, I.V. K. Freitas, A. Vieira, G. Gonçalves Lenzi, A.M.T. Silva, J.L. Faria, H.T. Gomes, Carbon nanomaterials from polyolefin waste: effective catalysts for quinoline degradation through catalytic wet peroxide oxidation, Catalysts 13 (9) (2023) 1259, https://doi.org/10.3390/catal13091259.
[23] J.L. Diaz de Tuesta, B. F. Machado, P. Serp, A.M. T. Silva, J.L. Faria, H. T. Gomes, Janus amphiphilic carbon nanotubes as Pickering interfacial catalysts for the treatment of oily wastewater by selective oxidation with hydrogen peroxide, Catal. Today 356 (2020) 205–215, https://doi.org/10.1016/j.cattod.2019.07.012.
[24] J.V. Gulmine, P.R. Janissek, H.M. Heise, L. Akcelrud, Polyethylene characterization by FTIR, Polym. Test. 21 (5) (2002) 557–563, https://doi.org/10.1016/s0142-9418(01)00124-6.
[25] S. Morales-Torres, T.L. Silva, L.M. Pastrana-Martinez, A.T. Brandao, J. L. Figueiredo, A.M. Silva, Modification of the surface chemistry of single- and multi-walled carbon nanotubes by HNO3 and H2SO4 hydrothermal oxidation for application in direct contact membrane distillation, Phys. Chem. Chem. Phys. 16 (24) (2014) 12237–12250, https://doi.org/10.1039/c4cp00615a.
[26] D.R. Lima, A. Hosseini-Bandegharaei, P.S. Thue, E.C. Lima, Y.R.T. de Albuquerque, G.S. dos Reis, C.S. Umpierres, S.L.P. Dias, H.N. Tran, Efficient acetaminophen removal from water and hospital effluents treatment by activated carbons derived from Brazil nutshells, Colloids Surf. A Physicochem. Eng. Asp. 583 (2019), https://doi.org/10.1016/j.colsurfa.2019.123966.
[27] R.S. Ribeiro, R.O. Rodrigues, A.M.T. Silva, P.B. Tavares, A.M.C. Carvalho, J. L. Figueiredo, J.L. Faria, H.T. Gomes, Hybrid magnetic graphitic nanocomposites towards catalytic wet peroxide oxidation of the liquid effluent from a mechanical biological treatment plant for municipal solid waste, Appl. Catal. B Environ. 219 (2017) 645–657, https://doi.org/10.1016/j.apcatb.2017.08.013.
[28] D. Yao, H. Yang, H. Chen, P.T. Williams, Co-precipitation, impregnation and so-gel preparation of Ni catalysts for pyrolysis-catalytic steam reforming of waste plastics, Appl. Catal. B Environ. 239 (2018) 565–577, https://doi.org/10.1016/j.apcatb.2018.07.075.
[29] A.H.R. Palser, Interlayer interactions in graphite and carbon nanotubes, Phys. Chem. Chem. Phys. 1 (18) (1999) 4459–4464, https://doi.org/10.1039/a905154f.
[30] J. Chen, X. Xu, L. Zhang, S. Huang, Controlling the diameter of single-walled carbon nanotubes by improving the dispersion of the uniform catalyst nanoparticles on substrate, Nano-Micro Lett. 7 (4) (2015) 353–359, https://doi.org/10.1007/s40820-015-0050-8.
[31] E.F. Kukovitsky, S.G. L'Vov, N.A. Sainov, V.A. Shustov, L.A. Chernozatonskii, Correlation between metal catalyst particle size and carbon nanotube growth, Chem. Phys. Lett. 355 (5-6) (2002) 497–503, https://doi.org/10.1016/s0009-2614(02)00283-x.
[32] J.H. Lehman, M. Terrones, E. Mansfield, K.E. Hurst, V. Meunier, Evaluating the characteristics of multiwall carbon nanotubes, Carbon 49 (8) (2011) 2581–2602, https://doi.org/10.1016/j.carbon.2011.03.028.
[33] A.G. Bannov, M.V. Popov, P.B. Kurmashov, Thermal analysis of carbon nanomaterials: advantages and problems of interpretation, J. Therm. Anal. Calorim. 142 (1) (2020) 349–370, https://doi.org/10.1007/s10973-020-09647-2.
[34] H. Li, N. Zhao, C. He, C. Shi, X. Du, J. Li, Thermogravimetric analysis and TEM characterization of the oxidation and defect sites of carbon nanotubes synthesized by CVD of methane, Mater. Sci. Eng. A 473 (1-2) (2008) 355–359, https://doi.org/10.1016/j.msea.2007.04.003.
[35] D. Bom, R. Andrews, D. Jacques, J. Anthony, B. Chen, M.S. Meier, J.P. Selegue, Thermogravimetric analysis of the oxidation of multiwalled carbon nanotubes: evidence for the role of defect sites in carbon nanotube chemistry, Nano Lett. 2 (6) (2002) 615–619, https://doi.org/10.1021/nl020297u.
[36] A. Tribalis, G. Panagiotou, K. Bourikas, L. Sygellou, S. Kennou, S. Ladas, A. Lycourghiotis, C. Kordulis, Ni catalysts supported on modified alumina for diesel steam reforming, Catalysts 6 (1) (2016), https://doi.org/10.3390/catal6010011.
[37] A.K. Sharma, S. Desnavi, C. Dixit, U. Varshney, A. Sharma, Extraction of Nickel nanoparticles from electroplating waste and their application in production of bio-diesel from biowaste, Int. J. Chem. Eng. Appl. 6 (3) (2015) 156–159, https://doi.org/10.7763/ijcea.2015.V6.472.
[38] I. Jastrzębska, J. Szczerba, P. Stoch, A. Błachowski, K. Ruebenbauer, R. Prorok, E. Śnieżek, Crystal structure and Mössbauer study of FeAl2O4, Nukleonika 60 (1) (2015) 47–49, https://doi.org/10.1515/nuka-2015-0012.
[39] C. Ragupathi, J.J. Vijaya, L.J. Kennedy, Synthesis, characterization of nickel aluminate nanoparticles by microwave combustion method and their catalytic properties, Mater. Sci. Eng. B 184 (2014) 18–25, https://doi.org/10.1016/j.mseb.2014.01.010.
[40] H. Muroyama, R. Nakase, T. Matsui, K. Eguchi, Ethanol steam reforming over Ni-based spinel oxide, Int. J. Hydrog. Energy 35 (4) (2010) 1575–1581, https://doi.org/10.1016/j.ijhydene.2009.12.083.
[41] J. Guo, H. Jiang, Y. Teng, Y. Xiong, Z. Chen, L. You, D. Xiao, Recent advances in magnetic carbon nanotubes: synthesis, challenges and highlighted applications, J. Mater. Chem. B 9 (44) (2021) 9076–9099, https://doi.org/10.1039/d1tb01242h.
[42] X. Wang, Z. Zhao, J. Qu, Z. Wang, J. Qiu, Fabrication and characterization of magnetic Fe3O4–CNT composites, J. Phys. Chem. Solids 71 (4) (2010) 673–676, https://doi.org/10.1016/j.jpcs.2009.12.063.
[43] K. Djebaili, Z. Mekhalif, A. Boumaza, A. Djelloul, XPS, FTIR, EDX, and XRD analysis of Al2O3Scales grown on PM2000 alloy, J. Spectrosc. 2015 (2015) 1–16, https://doi.org/10.1155/2015/868109.
[44] V. Tucureanu, A. Matei, A.M. Avram, FTIR spectroscopy for carbon family study, Crit. Rev. Anal. Chem. 46 (6) (2016) 502–520, https://doi.org/10.1080/10408347.2016.1157013.
[45] A. Misra, P.K. Tyagi, P. Rai, D.S. Misra, FTIR spectroscopy of multiwalled carbon nanotubes: a simple approach to study the nitrogen doping, J. Nanosci. Nanotechnol. 7 (6) (2007) 1820–1823, https://doi.org/10.1166/jnn.2007.723.
[46] B. Scheibe, E. Borowiak-Palen, R.J. Kalenczuk, Oxidation and reduction of multiwalled carbon nanotubes — preparation and characterization, Mater. Charact. 61 (2) (2010) 185–191, https://doi.org/10.1016/j.matchar.2009.11.008.
[47] E.C. Choi, W.S. Choi, B. Hong, The variation of surface contact angles according to the diameter of carbon nanotubes, J. Nanosci. Nanotechnol. 9 (6) (2009) 3805–3809, https://doi.org/10.1166/jnn.2009.ns71.
[48] T. Sun, B.D. Levin, J.J. Guzman, A. Enders, D.A. Muller, L.T. Angenent, J. Lehmann, Rapid electron transfer by the carbon matrix in natural pyrogenic carbon, Nat. Commun. 8 (2017) 14873, https://doi.org/10.1038/ncomms14873.
[49] Z.X.Li Tao, Ruilun Wang, Shuangyin Wang, Carbon-Based, Metal-Free Electrocatalysts for Renewable Energy Technologies, in: L. Dai (Ed.), Carbon-Based Metal-Free Catalysts: Design and Applications, I, Wiley-VCH, Weinheim, Germany, 2018, https://doi.org/10.1002/9783527811458.vol2-ch1.
[50] H. Liang, C. Zhu, A. Wang, K. Palanisamy, F. Chen, Facile synthesis of NiAl(2)O(4)/g-C(3)N(4) composite for efficient photocatalytic degradation of tetracycline, J. Environ. Sci. (China) 127 (2023) 700–713, https://doi.org/10.1016/j.jes.2022.06.032.
[51] L. Xu, X. Zhang, J. Han, H. Gong, L. Meng, X. Mei, Y. Sun, L. Qi, L. Gan, Degradation of emerging contaminants by sono-Fenton process with in situ generated H(2)O(2) and the improvement by P25-mediated visible light irradiation, J. Hazard Mater. 391 (2020) 122229, https://doi.org/10.1016/j.jhazmat.2020.122229.
[52] R. Zhu, Y. Zhu, H. Xian, L. Yan, H. Fu, G. Zhu, Y. Xi, J. Zhu, H. He, CNTs/ferrihydrite as a highly efficient heterogeneous Fenton catalyst for the degradation of bisphenol A: the important role of CNTs in accelerating Fe(III)/Fe(II) cycling, Appl. Catal. B Environ. 270 (2020), https://doi.org/10.1016/j.apcatb.2020.118891.
[53] F. Ghanbari, A. Hassani, S. Wacławek, Z. Wang, G. Matyszczak, K.-Y.A. Lin, M. Dolatabadi, Insights into paracetamol degradation in aqueous solutions by ultrasound-assisted heterogeneous electro-Fenton process: key operating parameters, mineralization and toxicity assessment, Sep. Purif. Technol. 266 (2021), https://doi.org/10.1016/j.seppur.2021.118533.
[54] M. Martin-Martinez, B.F. Machado, P. Serp, S. Morales-Torres, A.M.T. Silva, J. L. Figueiredo, J.L. Faria, H.T. Gomes, Carbon nanotubes as catalysts for wet peroxide oxidation: the effect of surface chemistry, Catal. Today 357 (2020) 332–340, https://doi.org/10.1016/j.cattod.2019.03.014.
[55] R.S. Ribeiro, A.M.T. Silva, J.L. Figueiredo, J.L. Faria, H.T. Gomes, The influence of structure and surface chemistry of carbon materials on the decomposition of

hydrogen peroxide, Carbon 62 (2013) 97–108, https://doi.org/10.1016/j.carbon.2013.06.001.
[56] N. Thomas, D.D. Dionysiou, S.C. Pillai, Heterogeneous Fenton catalysts: a review of recent advances, J. Hazard Mater. 404 (Pt B) (2021) 124082, https://doi.org/10.1016/j.jhazmat.2020.124082.
[57] X. Ou, H. Daly, X. Fan, S. Beaumont, S. Chansai, A. Garforth, S. Xu, C. Hardacre, High-ionic-strength wastewater treatment via catalytic wet oxidation over a $MnCeO_x$ catalyst, ACS Catal. 12 (13) (2022) 7598–7608, https://doi.org/10.1021/acscatal.2c01952.
[58] J.L. Diaz De Tuesta, F.F. Roman, V.C. Marques, A.S. Silva, A.P.F. Silva, T.C. Bosco, A.A. Shinibekova, S. Aknur, M.S. Kalmakhanova, B.K. Massalimova, M. Arrobas, A. M.T. Silva, H.T. Gomes, Performance and modeling of Ni(II) adsorption from low concentrated wastewater on carbon microspheres prepared from tangerine peels by FeCl3-assisted hydrothermal carbonization, J. Environ. Chem. Eng. 10 (5) (2022), https://doi.org/10.1016/j.jece.2022.108143.
[59] J. Zhang, B. Xin, C. Shan, W. Zhang, D.D. Dionysiou, B. Pan, Roles of oxygen-containing functional groups of O-doped g-C3N4 in catalytic ozonation: quantitative relationship and first-principles investigation, Appl. Catal. B: Environ. 292 (2021), https://doi.org/10.1016/j.apcatb.2021.120155.
[60] H.T. Gomes, S.M. Miranda, M.J. Sampaio, J.L. Figueiredo, A.M.T. Silva, J.L. Faria, The role of activated carbons functionalized with thiol and sulfonic acid groups in catalytic wet peroxide oxidation, Appl. Catal. B Environ. 106 (3-4) (2011) 390–397, https://doi.org/10.1016/j.apcatb.2011.05.044.
[61] H. Bai, P. He, L. Hao, Z. Fan, R. Niu, T. Tang, J. Gong, Waste-treating-waste: upcycling discarded polyester into metal–organic framework nanorod for synergistic interfacial solar evaporation and sulfate-based advanced oxidation process, Chem. Eng. J. 456 (2023), https://doi.org/10.1016/j.cej.2022.140994.
[62] V.A. Juwar, A.P. Rathod, Catalytic ozonation of real food wastewater using catalyst synthesized from waste, Environ. Technol. 44 (1) (2023) 12–21, https://doi.org/10.1080/09593330.2021.1961873.